CHAPTER 16

PHOTOSTABILITY AND PHOTOREACTIVITY IN BIOMOLECULES: QUANTUM CHEMISTRY OF NUCLEIC ACID BASE MONOMERS AND DIMERS

LUIS SERRANO-ANDRÉS* AND MANUELA MERCHÁN

Instituto de Ciencia Molecular, Universitat de València, Apartado 22085, ES-46071 Valencia, Spain

Abstract: The great potentials of high-level ab initio methods, in particular, the CASPT2//CASSCF protocol, are fully illustrated through: (i) the study of ultrafast energy relaxation in DNA/RNA base monomers, (ii) the intrinsic population mechanism of the lowest triplet state, and (iii) how bioexcimers can be considered as precursors of charge transfer and photoinduced reactivity. In order to describe these processes properly, the presence of conical intersections (CIs) and the topology of the involved pathways have to be determined correctly. Thus, in theoretical calculations the dynamic electronic correlation has to be considered. The accessibility of the CIs (or the seam of CIs) becomes crucial to understand the theoretical foundations of the overall photochemistry of the system. It is shown that from the minimum energy path (MEP) computed for the spectroscopic $\pi\pi^*$ excited state for the five natural nucleic acid bases, i.e., uracil, thymine, cytosine, adenine, and guanine, the system ultimately reaches in a direct fashion a CI connecting the initially excited state and the respective ground state, where a distorted out-of-plane ethene-like structure is obtained. Such CI can be seen as the basic feature responsible for the known photostability of the genetic material. Along the internal conversion processes, efficient singlet-triplet crossings are made apparent by the favorable intersystem crossing (ISC) mechanism. Similarly, it is concluded that the ultrafast electron transfer taking place in photosynthetic reaction centers can essentially be understood as a radiationless transition mediated by a CI. In addition, the photodimerization reaction of cytosine along the triplet manifold is mediated by a triplet-singlet crossing and it is revealed to be barrierless

Keywords: Ab Initio Calculations, Photobiology, Conical Intersections, DNA Photochemistry, Triplet Population

* Corresponding author, e-mail: Luis.Serrano@uv.es

M. K. Shukla, J. Leszczynski (eds.), Radiation Induced Molecular Phenomena in Nucleic Acids, 435–472.

16.1. INTRODUCTION: PHOTOBIOLOGY AND CONICAL INTERSECTIONS

From the perspective of a theoretical chemist, to get insight of a field like photobiology, the computation of the dynamics of the photochemical processes on the lowest potential energy hypersurfaces of biochromophores is of fundamental importance. The initial step to obtain an accurate representation of the potential energy surface of the excited state is a challenging objective by itself. It requires the use of advanced and computationally expensive quantum-chemical methods and strategies that are able to include, in a balanced way, the differential electronic correlation effects on the various electronic states under investigation. The dynamic path of the initially absorbed energy can then be followed along the complex topology of the hypersurface through favorable reaction paths, energy barriers, minima, and surface crossings, in a sequence of adiabatic and nonadiabatic processes which control the fate of the energy [1]. In the present chapter, we will focus on the accurate calculation of the excited states of different biochromophores, in particular, the nucleic acid bases. By computing reaction paths and stationary points on the DNA/RNA nucleobase monomers and dimers, we try to account for the rich photochemistry of the systems, both in the singlet and triplet mainfold. Ultrafast decay processes, which make the systems photostable upon UV-radiation, and the presence of excimers, i.e., excited dimers, as the precursors of charge transfer and photodimer formation in favorable internal conversion and intersystem crossing processes will be rationalized by using high-level accurate, predictive, multiconfigurational quantum chemical methods, in particular the CASPT2 and CASSCF approaches. We will discuss the role that multiconfigurational methods [2] play in the calculation of excited states hypersurfaces. It should be noted that they are the only reliable approaches available to deal with the description of general molecular situations. Particular emphasis will be given in analyzing the importance of including in a balanced way the differential correlation effects [3, 4], and the risks implicit in the use of low-level quantum chemical methods to describe photochemical reaction paths.

16.2. QUANTUM CHEMICAL METHODS: ELECTRONIC CORRELATION ENERGY AND MINIMUM ENERGY PATHS

As shall be discussed in next sections, the description of the topology of the potential energy hypersurfaces (PEHs) requires the use of high-level quantum-chemical methods and strategies [4, 5]. The differential effects of the correlation energy may have dramatic consequences in the determination of reaction profiles and location of state crossings. A nice theoretical photochemistry, even including reaction dynamics, but based on low-level PEHs descriptions may be totally spurious. The main problem arises due to the fact that energy gaps, reaction barriers, or the same existence of the crossing itself usually relies on the differential effects of the correlation energy, which typically require to be balanced by the use of high-quality methods and one-electron basis functions [3, 4]. Unfortunately, the

technologies needed to obtain all parameters such as geometries, energy profiles, electronic properties, coupling elements, etc., at the highest-level of theory are not yet fully developed, whereas, working within the Born-Oppenheimer approximation leads to a large number of problems in the crossing regions. Therefore, we must try to find a compromise between the different levels of theory used in the investigation and remember that the calculation of electronic energies for states of different nature requires a fully correlated method and balanced results. It does not matter how detailed is the characterization of the PEHs at the lower levels of theory, for instance, a conical intersection at the CIS or CASSCF levels, it is necessary to check if the conical intersection (CI) exists when the remaining correlation effects are included, or that the energy gaps and the topology of the PEHs is consistent with the photochemistry we are trying to model. The same applies when reaction dynamics at any order is going to be performed. The number of quantum chemical methods able to fully include correlation effects for all type of states and conditions is, however, quite limited [4, 5].

A second aspect of the studies on theoretical photochemistry is to determine the most adequate computational strategy for electronic structure calculations. It is by now clear the important role that CIs have in photochemistry [1, 6–8], but, as stated recently by Josef Michl: "*. . .in my opinion, too much emphasis has been put in recent years on the geometries of the lowest energy point of a conical intersection.* [. . .] *I would argue that these points are usually nearly irrelevant, because a molecule that has reached the seam of a conical intersection will fall to the lower surface right away and will not have time to ride the seam, looking for its lowest energy point. Thus, the effective funnel locations are those in which the seam is first reached, and not the lowest energy point in the intersection subspace*" [9]. Therefore, the question is now focused on the accessibility of the seam from the initially populated states, a complex task due to the multidimensionality of the problem. A reasonable choice, before proper dynamics can be performed and the minimum requirements in the description of the PEH can be established, is to compute minimum energy paths (MEPs) that inform about the reaction profile with no excess energy. Crucial hints will be obtained if proper and true MEPs are followed for the populated states, normally from the Franck-Condon (FC) region or from any other significant geometry, leading the computation toward states minima or directly to conical intersections, informing therefore about the presence or absence of energy barriers in the reaction path. Eventually, the accessibility of the seam from any of the points of the MEP can be also studied. As an example, next section reports excited states MEPs for DNA nucleobase monomers leading in a barrierless way to a crossing with the ground state which is not necessarily the lowest-energy CI. The methods and the specific computational strategies employed in the examples of this chapter are described in the next sections.

In the present study, optimizations of minima, transition states, PEH crossings, and minimum energy paths (MEPs) have been here performed initially at the CASSCF level of theory for all reported systems [2]. MEPs have been built as steepest descendent paths in a procedure [10] which is based on a modification of the

projected constrained optimization (PCO) algorithm of Anglada and Bofill [11] and follows the Müller-Brown approach [12]. Each step requires the minimization of the energy on a hyperspherical cross section of the PEH centered on the initial geometry and characterized by a predefined radius. The optimized structure is taken as the center of a new hypersphere of the same radius, and the procedure is iterated until the bottom of the energy surface is reached. Mass-weighted coordinates are used, such as the MEP coordinate corresponds to the so-called Intrinsic Reaction Coordinate (IRC) [10]. Regarding the conical intersection searches, they were performed using the restricted Lagrange multipliers technique as implemented in a modified version of the MOLCAS-6.0 package [13], in which the lowest-energy point was obtained under the restriction of degeneracy between the two included states. No nonadiabatic coupling elements were calculated.

At the computed CASSCF stationary points, CASPT2 calculations [14–17] on several singlet or triplet states were carried out to include the necessary dynamic correlation effects. In order to avoid weakly interacting intruder state problems, an imaginary level shift of 0.2 au has been included after careful testing [18]. The protocol is usually named CASPT2//CASSCF, and has proved its accuracy repeatedly [19–27]. In some cases, at the obtained CASSCF crossings and when the energy gaps at the CASPT2 level are too large (>2 kcal mol^{-1}), CASPT2 scans at close geometries were performed in order to find lowest-energy CASPT2 crossings which had the smallest energy difference between the relevant states. Different one-electron atomic basis sets were used, as indicated in each case, although a ANO-type basis set was required in some situations. Otherwise, 6-31G(d) or 6-31G(d,p) basis sets were employed. In general, the same basis set is used for energy optimizations and energy differences in order to obtain a balanced description of the PEH. No symmetry restrictions were imposed during the calculations. From the calculated CASSCF vertical transition dipole moments (TDM) and the CASPT2 band-origin energies, the radiative lifetimes have been estimated by using the Strickler-Berg relationship [28, 29]. Additional technical details can be found in each of the subsections. All calculations used the MOLCAS-6.0 set of programs [13].

16.3. ULTRAFAST ENERGY RELAXATION IN DNA/RNA BASE MONOMERS

Among the best well-known examples of photostability after UV radiation, the ultrafast nonradiative decay observed in DNA/RNA nucleobases, has attracted most of the attention both from experimental and theoretical viewpoints [30]. Since the quenched DNA fluorescence in nucleobase monomers at the room temperature was first reported [31] new advances have improved our knowledge on the dynamics of photoexcited DNA. Femtosecond pump-probe experiments in molecular beams have detected multi-exponential decay channels in the femtosecond (fs) and picosecond (ps) timescales for the isolated nucleobases [30, 32–34]. The lack of strong solvent effects and similar ultrafast decays obtained for nucleosides and nucleotides suggest that ultrashort lifetimes of nucleobases are intrinsic molecular properties, intimately

related to nonadiabatic dynamic processes leading to radiationless relaxation toward the ground state [30]. In modern photochemistry, the efficiency of nonradiative decays between different electronic states taking place in internal conversion processes is associated with the presence of crossings of different potential energy hypersurfaces in regions or seams of conical intersection points. These conical intersections (CIs) behave as energy funnels where the probability for nonadiabatic, nonradiative, jumps is high. Strongly quenched fluorescence and ultrafast nonradiative deactivation of the lowest spectroscopic state as measured in DNA/RNA nucleobases clearly points out the presence of an easily accessible conical intersection seam connecting the excited and the ground state potential energy surfaces.

The accurate theoretical characterization of the excited states of nucleobases at the FC geometry was accomplished for the first time a decade ago at the CASPT2 level of theory [35–37]. Some of the earliest attempts to characterize the geometrical structure of the low-lying excited states without symmetry restrictions at the CIS (Configuration Interaction Singles) level by Shukla and Mishra [38] yielded apparent state minima with strongly distorted out-of-plane conformations for the pyrimidine nucleobases, structures that were not initially identified as conical intersections. The first specific search of a CI in the isolated nucleobases was performed by Ismail et al. [39] at the CASSCF level of theory in cytosine, a study that suggested a population switch from the initial $\pi\pi^*$ to a $n_O\pi^*$ state followed by a deactivation through a conical intersection with the ground state $(gs/n_O\pi^*)_{CI}$. The importance of proper inclusion of correlation energy effects in such cases was highlighted by the first time in a following study of cytosine at the CASPT2 level by Merchán and Serrano-Andrés [3]. This study proved that the relative energy ordering of the excited states is dramatically changed upon the addition of dynamic correlation, and therefore the true nature of the CI in that region was a crossing of the ground and $\pi\pi^*$ states, $(gs/\pi\pi^*)_{CI}$, displaying a slight out-of-plane distorted ring and a elongated C=O bond length. The presence of another CI connecting the $\pi\pi^*$ and ground state in cytosine was found at the CIS level by Sobolewski and Domcke [40] in their study of the cytosine-guanine base pair. Such CI was determined as having a similar nature as that found in ethene by the elongation and twisting of the C_5C_6 double bond (Figure 16-1). Using a highly correlated method such as MRCI, Matsika has obtained the same type of ethene-like CI in uracil [41] and cytosine [42] by optimization of the $\pi\pi^*$ state. It is surprising that a low level method like CIS, lacking most of the correlation effects, was able to yield similar geometries, although not energies, than correlated methods, probably because just a HOMO-LUMO state was involved. Zgierski et al. [43, 44] reported ethene-like biradical CIs in cytosine and uracil upon geometry optimization with the CIS method. The same conical intersection was found for pyrimidine nucleobases at the DFT/MRCI [45] and CASPT2//CASSCF [46–48] levels of calculation, whereas the effects of solvation have been recently estimated [49]. Regarding purine nucleobases, the same type of conical intersection has been described for adenine [27, 50–54] and guanine [55, 56] at the DTF/MRCI and CASPT2//CASSCF levels of calculation. In this case, it is the twisting of the C_2N_3 bond which leads to a "ethene-like" CI.

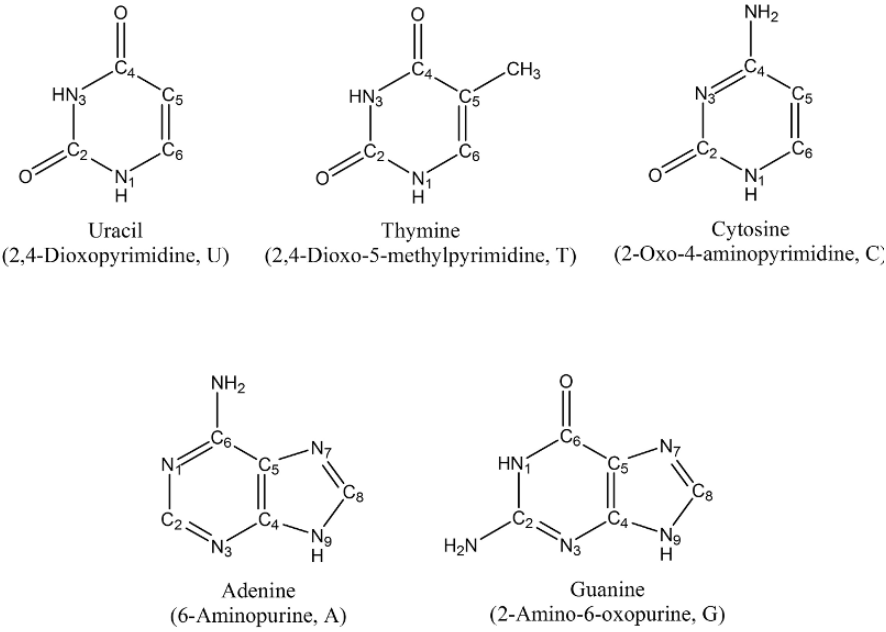

Figure 16-1. DNA and RNA nucleobases structure and labeling with their conventional name and, within parentheses, the IUPAC name and the abbreviation

In parallel to those determinations, Domcke, Sobolewski and coworkers [57, 58] found the existence of a new type of CIs between excited $\pi\sigma^*$ and ground states, in which the reaction coordinate for the relaxation of the system is the stretching and dissociation of a N-H bond. The relevance of this mechanism for the photostability of isolated nucleobase monomers is however unclear.

In fact, locating a conical intersection, computing its relative energy with respect to values at the FC geometry or minima, characterizing the nature of the CI, analyzing its nonadiabatic coupling elements, are very important tasks. Apart from the fact that in all cases the analysis has to be done at a proper level of theory, such effort might be useless if the actual accessibility of the CI seam is not studied. It is by now well recognized that a large number of CIs can be found for multidimensional systems in regions of the PEHs with a complex electronic state structure where degeneracy is frequent [59, 60]. Large number of state crossings takes place along different paths, many of which will be totally irrelevant for the photochemistry of the system. Properly mapping the PEH implies to estimate the accessibility of the CI, that is, to compute the energy barrier that must be surmounted to reach the funnel. Otherwise, if a CI represents the lowest energy of a given energy path, or even the lowest known CI of a system, the CI can be photochemically unimportant if a large energy barrier prevents the system to access such region of the PEH. Very few studies have been reported where the actual barriers have been accurately estimated

by computing the true minimum energy paths (MEPs) and transition states (TSs). In particular, the calculation of a MEP is quite often a cumbersome and expensive task, but it is unavoidable to get proper reaction profile. In DNA/RNA nucleobase monomers, and to the best of our knowledge, MEPs have been only reported up to now at the CASPT2//CASSCF level by Merchán, Serrano-Andrés, and coworkers for the pyrimidine nucleobases [47, 61] and adenine [27, 50], and by Blancafort and coworkers for cytosine [46] and adenine [51], whereas the present contribution summarizes the first report of a MEP for guanine which will be soon published [62]. In other studies just simple geometry optimizations, gradient-driven pathways, linear interpolations or relaxed scans have been carried out, and these strategies do not guarantee the presence or absence of energy barriers., or they can even yield in certain cases unconnected and therefore useless reaction paths. Among all the performed MEPs the most relevant ones lead the system on the initially populated singlet excited state at the FC geometry directly and in a barrierless way to a low-lying CI with the ground state. The absence of energy barriers explains the ultrafast (fs) decay measured in the nucleobases and allows joining them in a unified model. One interesting example is the guanine molecule. Whereas the studies reported previously for guanine [55, 67] do not include minimum energy paths, the model we suggest here is based on CASPT2//CASSCF calculations including MEPs [62]. As shown below, the five nucleobases have MEPs along the spectroscopic state leading in a barrierless form from the FC region to a CI with the ground state, $(gs/\pi\pi^*)_{CI}$. In the line of the words by J. Michl quoted in Section 16.2, it is worth mentioning that when the system reaches the crossing found along the MEP, belonging or close to the seam of CIs, the nonadiabatic jump to the lower surface becomes highly favorable. Apart from such crossing, computed adiabatically at 4.3 eV in guanine, we have located the lowest-energy CI at 4.0 eV with a similar structure, a conformation expected to play a less important role than the previous one.

Table 16-1 summarizes results obtained for the low-lying singlet states of the five natural DNA/RNA nucleobases: uracil (U), thymine (T), cytosine (C), adenine (A), and guanine (G). Information is compiled on vertical absorption energies, oscillator strengths, adiabatic band origins, vertical emissions, radiative lifetimes, and relative positions of the CI of the lowest $^1(\pi\pi^*)$ and ground states, computed at the crossing point with the end of the MEP $^1(\pi\pi^*)$ state. The final level of the calculations for the pyrimidine nucleobases is CASPT2//CASSCF(14,10)/ANO-S C, N, O [3s2p1d] / H [2s1p], whereas the purine nucleobases are computed at the CASPT2//CASSCF(16,13)/6-31G(d,p) level. More details can be found in the previous subsection and in the original publications [47, 50, 61].

The photochemistry of DNA and RNA nucleobases begins with the absorption of the energy to the bright $^1(\pi\pi^*$ HL) singlet state, computed vertically at 5.02 (U), 4.89 (T), 4.41 (C), 5.35 (A), and 4.93 (G) eV, with related oscillator strengths ranging from 0.053 (for C) to 0.436 (for U). These results are in near agreement with previous theoretical and gas-phase experimental data at 5.1 (U), 4.8 (T), 4.6 eV (C), 5.2 (A), and 4.6 eV (G) [35–37]. In cytosine and guanine the bright state is the lowest singlet state, unlike in the other systems. Direct absorption to other close-lying $n\pi^*$

Table 16-1. Computed spectroscopic properties for the low-lying singlet excited states of DNA/RNA base monomers at the CASPT2//CASSCF level of calculation[a]

States	Absorption		Emission			
	VA	f	T_e	VE	τ_{rad}	$(gs/\pi\pi^*)_{CI}$
			Cytosine			
$^1(\pi\pi^*$ HL)	4.41	0.053	3.62	2.4	29	3.6
$^1(n_O\pi^*)$	4.80	0.003	3.82	1.7	326	
$^1(n_N\pi^*)$	5.06	0.006				
			Thymine			
$^1(n_O\pi^*)$	4.77	0.004	4.05	3.3	2501	
$^1(\pi\pi^*$ HL)	4.89	0.167	4.49	3.8	9	4.0
$^1(\pi\pi^*)$	5.94	0.114				
			Uracil			
$^1(n_O\pi^*)$	4.88	0.003	4.03	3.2	2980	
$^1(\pi\pi^*$ HL)	5.02	0.436	4.53	3.9	9	3.9
$^1(\pi\pi^*)$	5.92	0.083				
			Adenine			
$^1(n_N\pi^*)$	4.96	0.004	4.52	2.8	334	
$^1(\pi\pi^*)$	5.16	0.004	4.83	4.6	251	
$^1(\pi\pi^*$ HL)	5.35	0.175				4.1
			Guanine			
$^1(\pi\pi^*$ HL)	4.93	0.209				4.3
$^1(n_O\pi^*)$	5.54	0.010	4.56	2.7	572	
$^1(\pi\pi^*)$	5.77	0.118	5.10	4.6	7	

[a]Basis set ANO-S C,N,O [3s2p1d]/H [2s] for cytosine, thymine, and uracil. Basis set 6-31G(d,p) for adenine and guanine. VA: vertical absorption, VE: vertical emission. Energies in eV, lifetimes in ns. Adiabatic energy difference for $(gs/\pi\pi^*)_{CI}$.

or $\pi\pi^*$ states is essentially forbidden, since the corresponding oscillator strengths are computed to be exceedingly small. These states will be populated only by internal conversion processes taking place along the main relaxation route of the $^1(\pi\pi^*$ HL) state. They are not expected to play major roles in the main photochemical event. After photoexcitation, the relaxation path along $^1(\pi\pi^*$ HL) in the five nucleobase systems leads, in a barrierless form, to the ethene-like conical intersection $(gs/\pi\pi^*)_{CI}$ in which the hydrogen atoms (or carbon in T and nitrogen in G) display a dihedral angle near 120° (see Figures 16-1 and 16-2), with the CI lying adiabatically (from the ground-state minimum) at 3.9 (U), 4.0 (T), 3.6 (C), 4.1 (A), and 4.3 eV (G). Most of the absorbed energy will decay nonradiatively to the ground state through the $(gs/\pi\pi^*)_{CI}$funnel in an ultrafast relaxation process that we assign to the femtosecond (fs) component of the multi-exponential decay measured in molecular beams at 130, 105, 160, 100 and 148 fs for U, T, C A and G [33], respectively. Figures 16-3 and 16-4 illustrate the key photochemical events taking place in pyrimidine and in purine nucleobases, respectively, i.e., the ultrafast decay of excited systems as an intrinsic molecular property based on the barrierless character of the main reaction path. We can confirm a very interesting conclusion from our studies of five natural

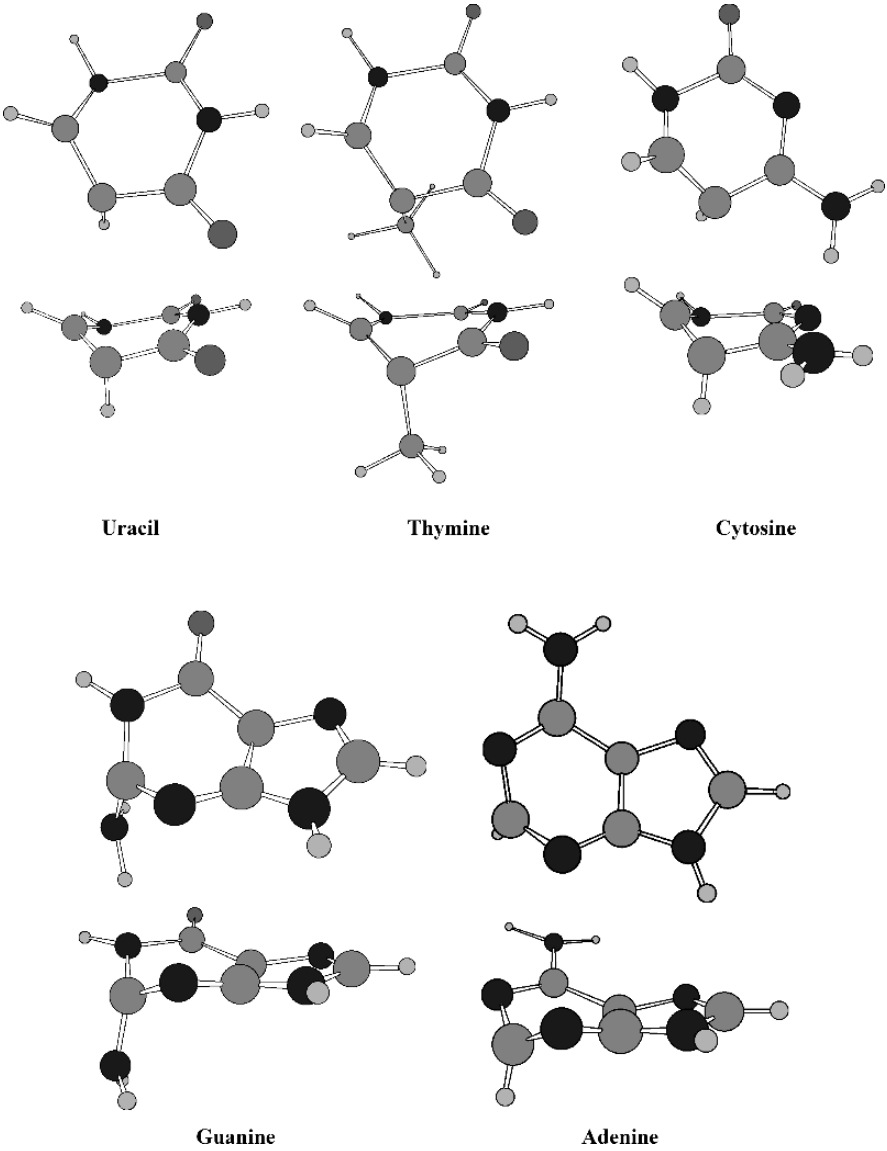

Figure 16-2. Optimized structures for the ethene-like $(gs/\pi\pi^*)_{CI}$ conical intersections for the five natural DNA/RNA base monomers

DNA/RNA nucleobases and several tautomers and derivatives that only the natural systems have barrierless MEPs connecting the FC region to the $(gs/\pi\pi^*)_{CI}$. In all the other studied purine derivatives, we have found different minima and energy barriers along the $^1(\pi\pi^*$ HL) MEP and thus hindering the ultrafast relaxation.

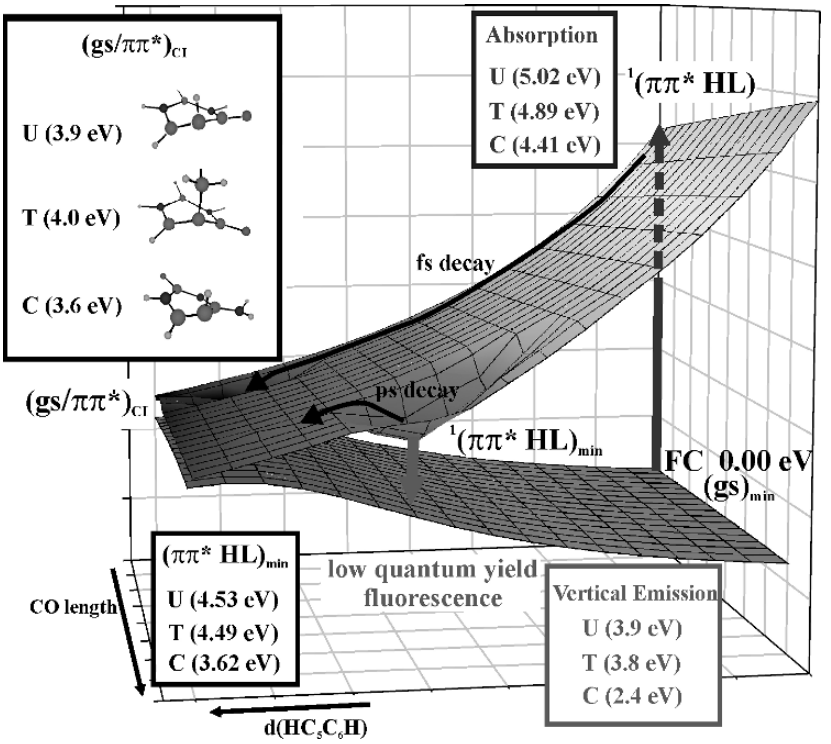

Figure 16-3. Global picture of the photochemistry of uracil (U), thymine (T), and cytosine (C) as suggested by the CASPT2 calculations**.** (Reproduced from Ref. [47] with permission from the American Chemical Society)

Such conclusion points toward the five nucleobases as the best outcome of natural selection for the genetic material that could become more stable upon UV radiation, especially prodigal in the early stages of life on Earth.

The photochemistry of the systems is however more complex and involves other states and additional paths. In particular, we propose a two- and three-state model for pyrimidine and purine nucleobases, respectively, to account for the basic photochemical phenomena observed in the systems upon absorption of UV light, including, at least, a fs and a ps decays, and extremely low fluorescence quantum yields in solution [31, 47, 49, 50, 63–65]. While most of the absorbed energy decays rapidly following the barrierless reaction path toward the ethene-like CI and the ground state, other low-lying accessible states will also be populated by internal conversion or intersystem crossing processes, either through the crossings of such states with the initially populated one or thanks to the excess energy of the system. We leave the discussion about population of triplet states for Section 16.4. Regarding the singlet manifold, in the pyrimidine nucleobases one $\pi\pi^*$ and one $n_O\pi^*$ low-lying excited states control the basic photochemistry of the system. The

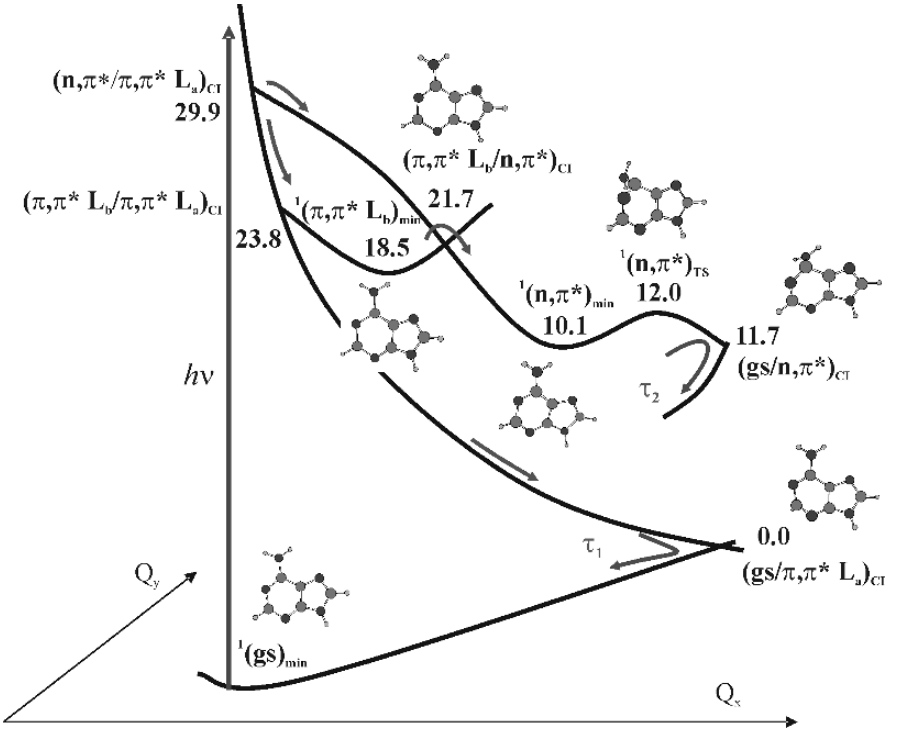

Figure 16-4. Scheme proposed, based on CASPT2 calculations, for the main decay pathways of adenine (A), measured in molecular beams with intrinsic lifetimes $\tau_1 < 100$ fs and $\tau_2 \sim 1$ ps. Energies in kcal mol^{-1} referred to the lowest conical intersection. A similar scheme is proposed for guanine (G). (Reproduced from Ref. [50] with permission from Wiley-VCH Verlag)

role of the $n_O\pi^*$ state is not fully elucidated. Whereas in U and T at the FC geometry the state is basically degenerate with the $\pi\pi^*$ state, its local planar minimum is considerably lower. Although not populated directly in the absorption process (its related oscillator strength is 20–40 times smaller than that of the $\pi\pi^*$ state), part of the energy can be transferred in the region where the crossing with the bright state takes place (see Figures 16-5 and 16-6). CIs connecting $n_O\pi^*$ and ground states have been estimated to lie too high in thymine, near 7.0 eV [48]. If such is the case they cannot be expected to play any important role in the measured deactivation processes in the gas phase. In solution, where longer decay lifetimes have been obtained, it has been proposed that a dark state, probably $n_O\pi^*$, is efficiently populated and behaves as a gateway for triplet state and photoproduct formation [66]. More promising to explain the gas-phase recordings are the CIs connecting also the $\pi\pi^*$ and ground states showing a different distortion that the ethene-like CI, such as the elongation of the C=O bond, $(gs/\pi\pi^*)_{CI(C=O)}$, or the twisting of the C_4N_3 bond, $(gs/\pi\pi^*)_{CI(sofa)}$, computed so far only for cytosine and derivatives [3, 42, 46], where reaching this CI from the bright $\pi\pi^*$ state means to surmount a

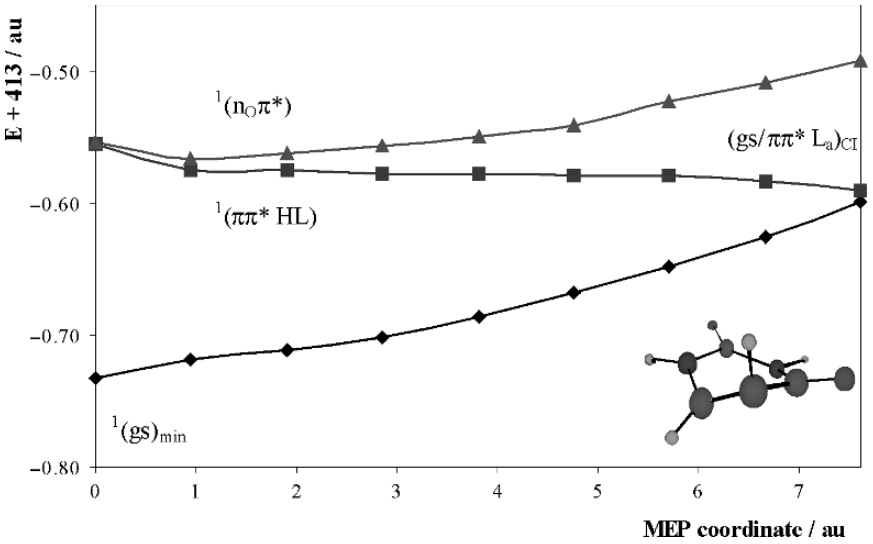

Figure 16-5. Evolution of the ground and lowest singlet excited states for uracil (U) from the FC geometry along the $^1(\pi\pi^*$ HL) MEP. (Reproduced from Ref. [47] with permission from the American Chemical Society)

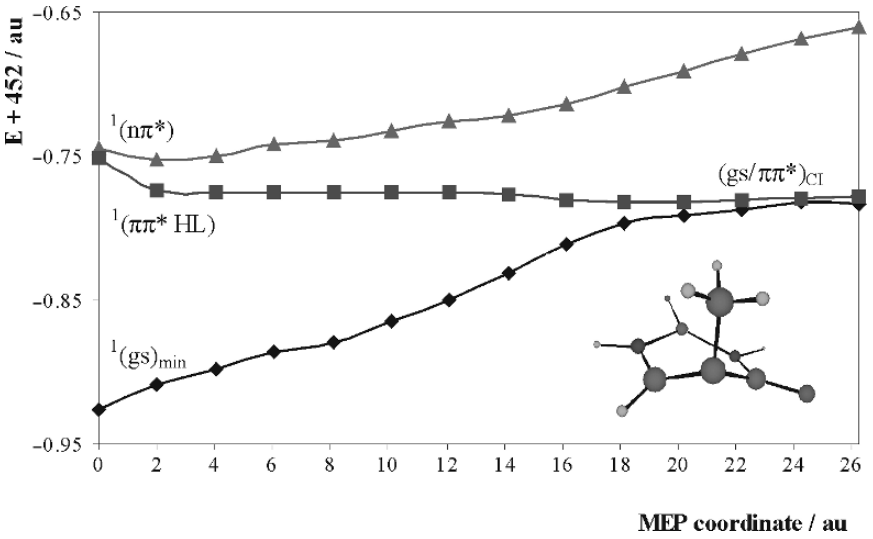

Figure 16-6. Evolution of the ground and lowest singlet excited states for thymine (T) from the FC geometry along the $^1(\pi\pi^*$ HL) MEP. (Reproduced from Ref. [47] with permission from the American Chemical Society)

few kcal mol^{-1} energy barrier from the $\pi\pi^*$ state minima, almost isoenergetic with all three (gs/$\pi\pi^*$) CIs. The computed barriers could explain the ps decay lifetime, as it occurs with the barrier computed in similar circumstances to reach another computed S_0-S_1 CI, $(gs/n_N\pi^*)_{CI}$ [3, 46].

The photochemistry of purines is more complex. First, because of the involvement of at least three low-lying excited states, one $n_N\pi^*$ (A) or $n_O\pi^*$ (G), and two $\pi\pi^*$ states, typically labeled $^1(\pi\pi^*\ L_a)$ or $^1(\pi\pi^*$ HL) (the HOMO-LUMO and bright state) and $^1(\pi\pi^*\ L_b)$. Second, because of the presence of near-degenerate molecular tautomers: 7H-9H, keto-enol, and imino [27, 30, 50, 67–71], and its different stability upon the polarity of the medium. For the natural 9H keto tautomer, we have recently proposed [27, 50] a three-state model for the photochemistry of adenine. A scheme is depicted in Figure 16-7. Whereas the $^1(\pi\pi^*\ L_a)$ state is responsible for absorption and ultrafast fs relaxation of the energy via the $(gs/\pi\pi^*)_{CI}$, as explained above, the $^1(\pi\pi^*\ L_b)$ and $n_N\pi^*$ states play a secondary role, being populated by excess energy processes and through respective CIs with the $^1(\pi\pi^*\ L_a)$ state. A second channel for energy was proposed involving $^1(\pi\pi^*\ L_b)$ and $n_N\pi^*$ states, interconnected through a CI, and a final deactivation toward the ground state through a conical intersection, $(gs/n_N\pi^*)_{CI}$, that we related with the second and slow ps decay found in molecular beams [30, 33]. Unlike in the pyrimidine nucleobases, where the weak fluorescence measured in solution [30, 31, 63–65] can be attributed to a local planar minimum belonging to the $^1(\pi\pi^*$ HL) PEH, no minimum was found for such state in adenine. Instead, the fluorescence is assigned to the S_1 $^1(\pi\pi^*$

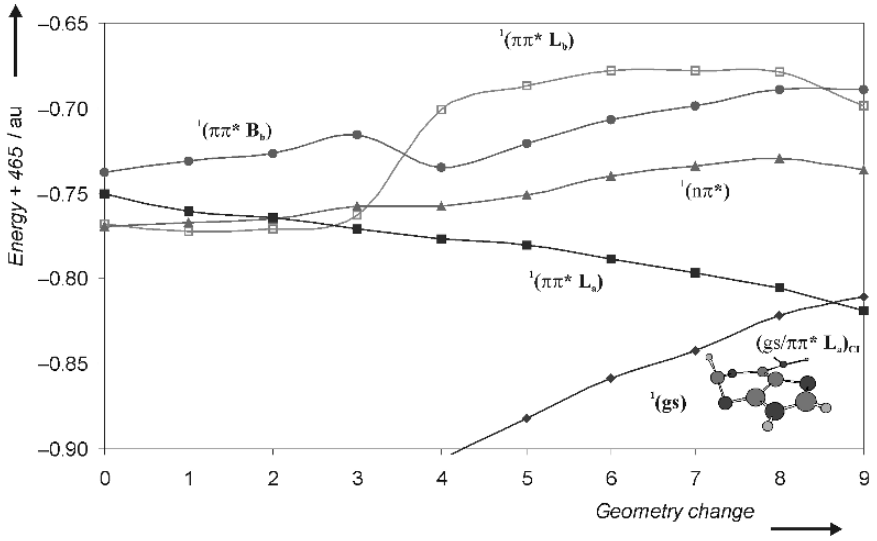

Figure 16-7. Evolution of the ground and lowest singlet excited states for adenine (A) from the FC geometry along the $^1(\pi\pi^*$ HL) MEP. (Reproduced from Ref. [50] with permission from Wiley-VCH Verlag)

L_b) planar minimum, and in particular for the isolated system to that of 7H-adenine, more stable than the natural 9H-tautomer [30, 50]. For guanine we propose a similar three-state scheme [62]. As in adenine, the MEP on the $^1(\pi\pi^*$ HL) state leads directly without any barrier to the ethene-like CI. The other two low-lying states $^1(\pi\pi^*$ L_b) and $n_O\pi^*$ play a secondary role and the latter is proposed as responsible for the ps decay trough the CI $(gs/n_O\pi^*)_{CI}$. The related distortion involves, in both purine nucleobases, the twisting of the C_6N_1 bond and a perpendicular NH_2 group (A) [27, 50] or carbonylic oxygen (G) [62]. Considering the $n\pi^*$ nature of the state involved, it can be expected that this relaxation path will be more perturbed in polar and protic solvents.

As we formulated above, the unified model presented for the main relaxation path of the nucleobase monomers is based not just on the existence of $(gs/\pi\pi^*)_{CI}$ at 0.6–1.1 eV below the $^1(\pi\pi^*$ HL) state at the FC region, but essentially on the barrierless character of the MEP computed from the latter to the former structures [47, 50, 61], which guarantees the accessibility of the seam at least along the path without excess energy. Assuring the barrierless character of the reaction path and the proper connection from the FC region to the CI is difficult, and it has a number of problems that we want to illustrate here, most of them related to the balanced nature of the calculations. Up to now, only multiconfigurational approaches have been able to cope with the description of the conical intersections and barrier heights in the excited states of nucleobases, although the accurate determination of the different pathways seems to depend on the amount of correlation energy employed. For instance, in U a CASSCF(10,8)/6-31G(d,p) (valence π space, 10 electrons distributed in 8 orbitals) geometry optimization of the $^1(\pi\pi^*$ HL) state starting at the FC geometry leads directly to a planar structure. After careful testing of the active space it was concluded that the addition of three extra active correlating orbitals was required to reach directly the ethene-like CI, *i.e.*, an active space CASSCF(10,11), in agreement with the results obtained with other highly correlated method like MRCI [41]. The same conclusion was obtained by increasing the quality of the basis set. Figure 16-5 contains the MEP performed for uracil at the CASPT2(14,10)//CASSCF(10,11)/ANO-S level of theory showing the barrierless profile of the $^1(\pi\pi^*$ HL) state pathway from FC to the ethene-like CI $(gs/\pi\pi^*)_{CI}$, related to the measured femtosecond decay, and representing the most efficient path for energy deactivation in nucleobases [47]. The addition of the three extra correlating orbitals was required to properly describe the steepest descendent character of the MEP in uracil, independently of the basis set, and it is surely related with the subtle balance of correlation energy effects that one can find when describing reaction profiles. The case of thymine also illustrates the complexity of the problem. For T, CASSCF geometry optimizations for the lowest $^1(\pi\pi^*$ HL) state using valence π active spaces and the 6-31G(d) or 6-31G(d,p) basis sets led directly from the FC region to the planar $^1(\pi\pi^*$ HL) state minimum, a local stationary point located in a totally different region of the hypersurface than the ethene-like CI. Just by improving the basis set to ANO-S quality however changed the outcome, and the optimization led to the ethene-like conical intersection instead. ANO-type

basis sets are known to be more accurate and get better account of the correlation energy. It is proved that they provide much better results that segmented basis sets with the same number of contracted functions [4, 5, 25]. Both improvements, increasing the quality of the basis set or adding extra correlating orbitals to the active space, partially compensate the lack of dynamic correlation energy of the π-valence CASSCF method. It is therefore clear that erroneous results can be obtained when using low levels of calculation for instance to perform molecular dynamics, where the outcome of the trajectory or the wave-packet propagation strongly relies on the PEH profile. In order to assure the barrierless character of the relaxation in thymine also, an equivalent MEP as in uracil, i.e., from the FC geometry leading to the ethene-like CI, has been computed and it is displayed in Figure 16-6 [47].

The complexity of the problem increases in the case of cytosine. The MEP computed for C at the CASSCF level (valence π space) shows no apparent energy barrier in going from the FC region toward a planar S_1 $^1(\pi\pi^*\ \mathrm{HL})_{\mathrm{min}}$ minimum [61]. Energy optimizations or MEPs adding extra correlating orbitals like that in uracil and thymine or improving the basis set do not change the outcome. It can be observed that cytosine has experimental behavior similar to other nucleobases [30, 33]. Therefore, we can question if the proposed model is valid or not in this case. Unlike the other systems, the two critical points namely the ethene-like CI $(\mathrm{gs}/\pi\pi^*)_{\mathrm{CI}}$ and the planar minimum $^1(\pi\pi^*\ \mathrm{HL})_{\mathrm{min}}$ in cytosine lie almost isoenergetic. Therefore, the description of the barriers heavily depends on subtle effects of the correlation level used in the optimization approach. Possibly a MEP calculation at the CASPT2 level, computationally not feasible by now, would solve the problem, although the presence of stationary points isoenergetic with the ethene-like CI clearly indicates that we cannot discard that the pathways to the planar $^1(\pi\pi^*\ \mathrm{HL})_{\mathrm{min}}$ minima play a competitive role for the energy relaxation. An evidence pointing out in that direction becomes clear when a linear interpolation in internal coordinates (LIIC) is performed between the optimized FC and $(\mathrm{gs}/\pi\pi^*)_{\mathrm{CI}}$ geometries in C [47]. Energy barriers of about 6.6 and 2.5 kcal mol^{-1} are obtained at the CASSCF and CASPT2 level of calculations, respectively, along the evolution of the path [47]. Inclusion of dynamical correlation clearly decreases the barrier height, which is found at the beginning of the interpolation, when the dihedral angle HC_5C_6H (see Figure 16-1) increases up to 16°. Typically, a barrier obtained along a linear interpolation, in particular if a tight set of points is employed, represents an upper bound for the actual barrier, even when the initial point here is the S_1 state at the FC geometry, a situation without excess energy. In this case a profile with a barrier expected lower than 2.5 kcal mol^{-1} should be considered essentially barrierless. The same type of LIICs performed in uracil and thymine yielded CASPT2 barriers of 5 and 12 kcal mol^{-1} at angles near 30 and 16°, respectively, which can be compared with the barrierless character of their MEPs [47]. Evidence also indicates the absence of barrier in cytosine if more accurate MEPs could be obtained. In any case, for cytosine it can be expected that the final resolution of the problem will have to wait until proper reaction dynamics can be performed on accurate PEHs. It is worth recalling that in adenine and in guanine the equivalent MEPs were

obtained barrierless even at the lowest levels the valence π CASSCF calculations, and 6-31G(d,p) basis sets employed here, (Figure 16-7) [27, 50, 62].

In summary, based on the calculation of MEPs, minima, transition states, and conical intersections, the present research yields a unified view to describe the main photochemical events such as the ultrafast subpicosecond decay and low fluorescence quantum yield in the five DNA/RNA natural nucleobases after UV irradiation. Two and three low-lying excited states for pyrimidine and purine nucleobases, respectively are the main responsible for the photochemistry of the systems. The main photochemical event, the ultrafast relaxation of the initially populated $^1(\pi\pi^*$ HOMO→LUMO) state, is explained by the barrierless path computed for the MEP connecting the FC region to the CI with the ground state. According to the present results, it seems that this behavior does only occur for the five natural nucleobases, whereas their main tautomers and derivatives have different relaxation profiles. On the other hand, measured longer lifetime decays and low quantum yield emission in the nucleobases are suggested to be connected to the presence of a $^1(\pi\pi^*)$ state planar minimum on the S_1 surface and the barriers to access other conical intersections. That minimum is the source of the weak emission recorded for the systems, although such planar structure and other close-lying excited states of $n\pi^*$ type are not expected to participate in the key photochemical event taking place along the main decay pathway toward the ethene-like CI, but to be involved in the slower relaxation paths. Finally, we have also shown the importance of the quantum chemical description of the PEH. The absence of dynamic electron correlation energy in a multiconfigurational procedure like CASSCF (in general the lack of correlation energy in any method) may easily lead to find spurious conical intersections and energy barriers along the different paths and miss the main relaxation pathway, as it has been shown for uracil and thymine. The use of low-level quantum-chemical methods, which may fortuitously lead to correct results, must be necessarily considered a high-risk procedure in photochemical studies, especially when the obtained PEHs are to be used for further reaction dynamics.

16.4. EFFICIENT POPULATION OF TRIPLET STATES

There is large number of processes in photobiology mediated by the population of the lowest triplet state of the biochromophore which is generally a long lived and highly reactive state [72]. There are many examples in which molecules in triplet states act as energy donors, for instance transferring its energy to other systems and behaving as photosensitizers, or give rise to effective reactivity. In any case, and considering that the primary step of the photochemical process after light absorption involves basically the population of the lowest singlet excited state (S_1), it is necessary to find those channels for energy deactivation and transfer in which the lowest triplet excited state (T_1) can be rapidly and efficiently populated through an intersystem crossing (ISC) mechanism. In initial studies at the semiempirical [73–75] and ab initio [76–78] levels, the ISC rates were typically estimated by computing the spin-orbit coupling (SOC) matrix elements between the singlet and

triplet states at the Franck-Condon (FC) structure. Thus the well-known qualitative El-Sayed rules [79, 80] that the coupling is the largest between alike states and forbidden otherwise for $\pi\pi^*$ and $n\pi^*$ states in organic molecules were obtained. Nowadays, it is possible to determine regions of close degeneracy between the states, singlet-triplet crossing regions, and compute the SOC elements, combining the two required conditions for efficient ISC: Small energy gaps and relatively large SOC elements. As compared to internal conversion (IC) processes, the regions of the PEHs for effective ISC are more extensive.

In the present report the SOC strength between selected CASSCF states was computed as

$$SOC_{lk} = \sqrt{\sum_{u} \left| \left\langle T_{l,u} \right| \hat{H}_{SO} \left| S_k \right\rangle \right|^2} \qquad u = x, y, z$$

which can be considered the length of the spin-orbit coupling vector SOC_{lk} with component $\left\langle T_{l,u} \right| \hat{H}_{SO} \left| S_k \right\rangle$. Also, from the calculated CASSCF transition dipole moments (TDM) and the CASPT2 excitation energies, the radiative lifetimes have been estimated by using the Strickler-Berg relationship [28, 29]. In particular, the singlet-triplet TDMs were obtained by the following expression [61]:

$$TDM_{ST} = \langle S | r^l | T^k \rangle = \sum_n \frac{\langle S^0 | r^l | S_n^0 \rangle \langle S_n^0 | H_{SO}^k | T^{k,0} \rangle}{E(T^0) - E(S_n^0)} + \sum_m \frac{\langle S^0 | H_{SO}^k | T_m^{k,0} \rangle \langle T_m^{k,0} | r^l | T^{k,0} \rangle}{E(S^0) - E(T_m^0)}$$

In the present chapter we will describe some examples in which barrierless minimum energy reaction paths along the potential hypersurfaces of several systems will be shown to connect initially excited singlet states with the triplet manifold. Those examples include the isoalloxazine molecule and different DNA nucleobases.

One typical case is the observed photoinduced electron-transfer to triplet flavins and flavoproteins [81, 82]. Proteins like phototropin act as blue-light sensitive photoreceptors that regulate phototropism response in higher plants. The triplet-state formation of the main chromophore, the single flavin mononucleotide (FMN), triggers the photochemical cycle of flavin-related compounds. A detailed account for the singlet-triplet non-radiative transfer in isoalloxazine, the flavin core ring (Figure 16-8), within the framework of nonadiabatic photochemistry has been recently provided [83]. In particular, the key issue is whether relaxation to the triplet state involves a direct coupling between the lowest singlet and triplet states or proceeds via a third excited state. In order to understand those aspects the low-lying singlet and triplet states of isoalloxazine have been computed and characterized. Geometries of the ground and low-lying valence excited states, minimum energy paths, conical intersections, and singlet-triplet states crossings were optimized at the CASSCF level [2]. A careful calibrated selection of the active space led to sixteen valence electrons distributed among thirteen valence MOs, resulting in CASSCF(16, 13) wave functions. The basis set 6-31G(d) was used throughout.

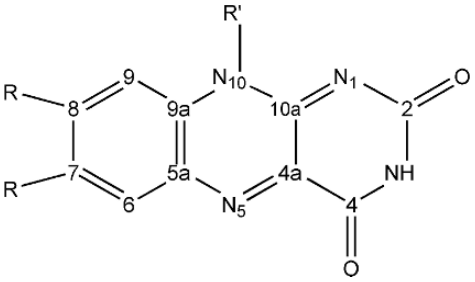

Figure 16-8. Structure and labeling of the isoalloxazine ring and related flavins. Isoalloxazine (benzo[g]pteridine-2,4(3H,10H)-dione): R = R' = H. FMN (Flavin mononucleotide): R = CH_3; R' = CH_2– $(CHOH)_3$–CH_2O–PO_3^{2-}

The photochemical process starts with the absorption of the energy by the molecule at its ground state equilibrium structure (FC). Table 16-2 compiles computed absorption and emission energies, oscillator strengths, and radiative lifetimes for the lowest energy states of isoalloxazine. Most of the energy in the absorption process will populate at low energies the state with the largest oscillator strength, that is the singlet $S_1\pi\pi^*$ state. Figure 16-9 displays a scheme of the evolution of the energy starting from the FC geometry and along the S_1 hypersurface following the corresponding MEP. Along the relaxation pathway on S_1, the first event is the occurrence of a near-degeneracy between S_1 and T_N, close at the FC region, leading to a singlet-triplet crossing denoted by $(S_1/T_N)_{STC}$. In the vicinity of such crossing the ISC mechanism is favorable in the two required aspects, that is, the close energetic proximity of both states and the relatively large SOCs. The computed electronic SOC around this region ranges from 2 to 11 cm^{-1}, reflecting the spin-orbit allowed character of the $^1(\pi,\pi^*)/^3(n,\pi^*)$ transition as enunciated by the qualitative El Sayed rules for intersystem crossing [79, 80, 84]. Further along the path the equilibrium structure of the lowest singlet excited state

Table 16-2. Computed absorption energies, band origins, vertical emissions, oscillator strengths (within parenthesis), and radiative lifetimes (τ_{rad}) for the low-lying singlet excited states of isoalloxazine

Vertical Transition (eV)			Band Origin (eV)		Emission (eV)		
State	CASSCF	CASPT2	CASSCF	CASPT2	CASSCF	CASPT2	τ_{rad}
Singlet states							
$\pi\pi^*$	4.15	3.09 (0.239)	3.20	2.69	2.21	2.04	15 ns
$n_N\pi^*$	4.79	3.34 (0.007)	3.82	3.33	2.65	2.61	467 ns
$n_O\pi^*$	5.15	3.75 (0.001)	3.52	3.16	2.19	2.33	6458 ns
Triplet states							
$\pi\pi^*$	3.14	2.52	2.41	2.03	1.73	1.75	116 ms
$n_N\pi^*$	4.30	2.97	3.50	2.73	3.00	2.37	
$n_O\pi^*$	4.99	3.70	3.40	3.10	2.20	2.34	

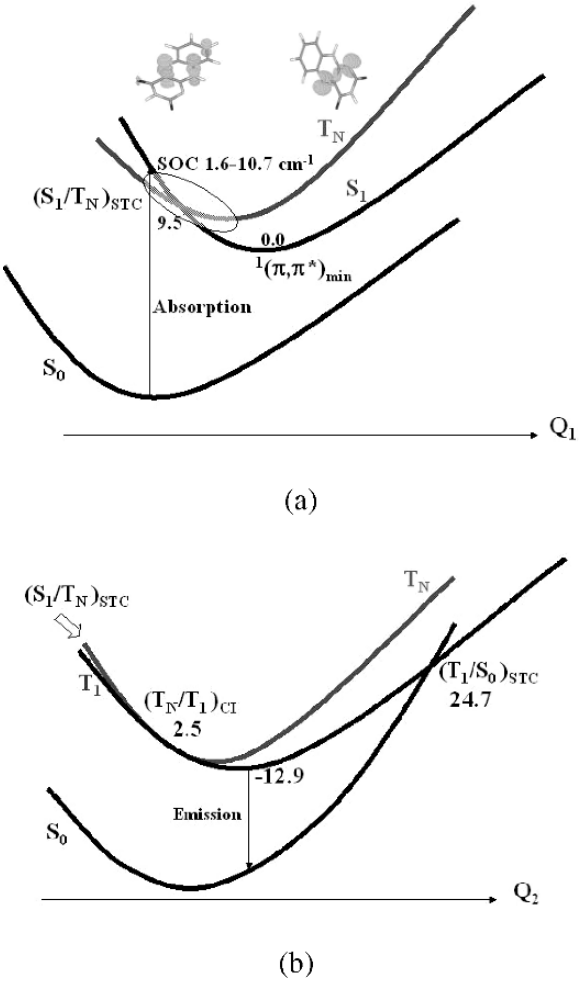

Figure 16-9. Schematic representation of the photochemical events after light absorption once isoalloxazine has been promoted vertically to S_1. (a) Population of T_N in the vicinity of Franck-Condon region by intersystem crossing mechanism. (b) Internal conversion toward T_1 mediated by the $(T_N/T_1)_{CI}$ leading ultimately to the $^3(\pi\pi^*)_{min}$ structure. Energies are in kcal·mol^{-1}. Q_1 and Q_2 are reaction coordinates. (Reproduced from Ref. [83] with permission from the American Chemical Society)

$^1(\pi,\pi^*)_{min}$ is ultimately reached. The initial steps of the photochemical mechanism after absorption of a photon involve the decay of its lowest singlet excited state S_1 in times shorter than the experimental time resolution to an intermediate related to T_N. The population transfer occurs before the S_1-minimum is encountered, which is consistent to the fact that the fluorescence quantum yield of the flavins compounds is lower than the intersystem crossing quantum yield and triplet state formation [85]. Polar solvents seem to increase ISC and decrease fluorescence quantum yields in

isoalloxazines [86, 87]. Accordingly to their nature, $S_1(\pi\pi^*)$ and T_N $(n\pi^*)$ states in polar media would be stabilized and destabilized, respectively, with respect to that in vacuo values, leading to a decrease in the vertical energy gap and a singlet-triplet crossing, which might occur closer to the FC region, favoring the trends observed experimentally.

Once the ISC process has taken place in the vicinity of the $(S_1/T_N)_{STC}$ crossing, it is possible to study the evolution of the system by computing a MEP along the $^3(n_N,\pi^*)$ state hypersurface. As summarized in Figure 16-9, once the T_N state is populated, a rapid T_N to T_1 internal conversion occurs, mediated by the $(T_N/T_1)_{CI}$ conical intersection, which is computed to be 2.5 kcal mol^{-1} (0.11 eV) above the $^1(\pi,\pi^*)_{min}$, the reference structure chosen for the relative energies depicted in Figure 16-8. The T_N-MEP leads ultimately to the equilibrium structure of the T_1 state, $^3(\pi,\pi^*)_{min}$, placed 12.9 kcal mol^{-1} (0.56 eV) below $^1(\pi,\pi^*)_{min}$. From the relaxed T_1 three different photochemical events can take place: emission (phosphorescence), reactivity of the long-lived T_1 isoalloxazine with different protein residues, and radiationless decay to the ground state through a conical intersection $(T_1/S_0)_{STC,}$ triggering the internal conversion to the ground state. To analyze the importance of this final internal conversion it is required to compute the energy barrier leading from the populated $^3(\pi,\pi^*)_{min}$ to the corresponding CI. Once the $(T_1/S_0)_{STC}$ structure was obtained, the barrier was found to be 37.6 kcal/mol at the CASPT2 level. Therefore, the deactivation of T_1-isoalloxazine to the ground state non-radiatively via the $(T_1/S_0)_{STC}$ crossing ultimately depends on the excess of vibrational energy in the system at this point, otherwise the molecule will just emit. As compiled in Table 16-2, the radiative lifetime for T_1 is of the order of 116 ms, consistent with the nature of state. On the other hand, it is known that after T_1 formation, the flavin core ring, chromophore of phototropin, reacts with the sulfur atom of the cysteine-39 to form an adduct [85]. Other systems also populate its triplet state efficiently and act as photosensitizers, and are prone to transfer its energy or react with other systems. One of these cases is that of the furocoumarines, like psoralen, in which mechanisms of triplet state population have been recently studied [88–90].

As a second example of intersystem crossing mechanism in biochromophores we include here the case of the DNA pyrimidine nucleobases, starting by the uracil molecule [91]. In previous sections we presented a model for the rapid internal conversion of the singlet excited rationalizes the ultrafast decay component observed in these systems, both in the gas phase and in solution. Despite the short lifetimes associated to this state, which is the main contributor to the photophysics of the system, formation of photodimers Pyr<>Pyr has been observed for the monomers in solution, as well as in solid state, for oligonucleotides, and DNA [92]. Since the sixties, the determination of the mechanism of the photoinduced formation of cyclobutane dimers has been the subject of numerous studies [92, 93–97]. One of the most classic models that has been proposed for the photodimerization of Pyr nucleobases in solution invokes photoexcitation of a molecule to a singlet state followed by population of a triplet state by an intersystem crossing mechanism

and subsequent reaction of the triplet Pyr with a second molecule in the ground state [92–98] (see Section 16.5). In particular, the presence of the triplet state of uracil in solution has been observed by using different experimental techniques, such as flash photolysis [99]. Indirect evidence for the involvement of a triplet state has also been provided by using specific triplet quenchers, as well as external photosensitizers [92, 93, 99]. In uracil the intersystem crossing quantum yield ϕ_{isc} is strongly dependent on the excitation wavelength in the lowest-energy absorption band. The value increases from 1.4×10^{-3} at 280 nm (4.43 eV) to 1.6×10^{-2} at 230 nm (5.39 eV) [92, 93].

By computing CASPT2//CASSCF minimum energy paths, singlet-triplet crossings, conical intersections, and state minima, it is possible to identify two different mechanisms in which the population can be transferred from the initially populated $^1(\pi\pi^*$ HL) state to the triplet manifold through respective singlet-triplet crossings (STC). It can be deduced from the Table 16-3 that the initial excitation at the FC region basically populates the low-lying $\pi\pi^*$ singlet state at 5.18 eV (S_2) due to the larger oscillator strength, even though the $n_O\pi^*$ state lies lower in energy at 4.93 eV. Also, it is common to find that the lowest triplet $^3(\pi\pi^*$ HL) state has much lower energy, vertically at 3.80 eV. Considering the large energy gap and the negligible SOC between the initially populated singlet $^1(\pi\pi^*$ HL) and the lowest energy triplet $^3(\pi\pi^*$ HL) T_1 state at the FC region, a direct transfer of population between both states is highly unlikely. It is necessary to find molecular structures which minimize energy gaps and maximize SOC elements. In initial studies on ISC processes [78] emphasis was focused on the vibronic effects on the SOCs. Those contributions were mainly reflecting the need to distort the geometry and find favorable regions for ISC.

By means of the calculation of the MEP on the $^1(\pi\pi^*$ HL) PEH of uracil as discussed in previous Section 16.2, two STC can be located. Figure 16-10 contains a scheme of the different mechanisms found in uracil for efficient population of the lowest triplet state based on computed MEPs and PEHs crossings. More details can be found elsewhere [91]. At the 4.6 eV along the MEP the STC $(^3n_O\pi^*/^1\pi\pi^*)_{STC}$

Table 16-3. Computed Spectroscopic Properties for the Low-Lying Singlet and Triplet Excited States of Uracil at the CASPT2//CASSCF(14/10)/6-31G(d,p) Level

State	Vertical Transition (eV)		Band Origin (T_e, eV)		
	CASSCF	CASPT2[a]	CASSCF	CASPT2	τ_{rad}
$^1(n_O\pi^*)$	5.18	4.93 (0.0006)	4.07	4.03	3051 ns
$^1(\pi\pi^*)$	6.82	5.18 (0.1955)	6.30[b]	4.48[b]	7 ns
$^1(\pi\pi^*)$	7.29	6.18 (0.0733)			
$^3(\pi\pi^*)$	3.98	3.80	3.16	3.15	135 ms
$^3(n_O\pi^*)$	4.87	4.71	3.81	3.91	
$^3(\pi\pi^*)$	5.76	5.33			

[a] Oscillator strength within parentheses; [b] Minimum optimized at the CASPT2 level.

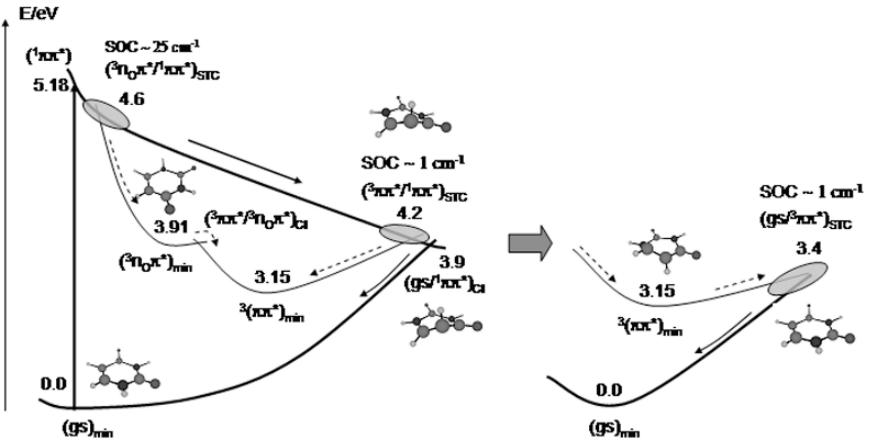

Figure 16-10. Scheme, based on CASPT2 results, of the photochemistry of uracil focused on the population of the lowest-energy triplet state. (Reproduced from Ref. [91] with permission from Elsevier.)

was revealed. At this point the molecule has a slight out-of-plane distortion and $^1(\pi\pi^*$ HL) state crosses the lowest triplet $^3n\pi^*$ state. As expected, the computed SOC is high ($\sim$25 cm^{-1}) and thus indicating to efficient ISC between the states. This first mechanism to populate the lowest $^3(\pi\pi^*$ HL) T_1 state in uracil is very similar to that described above for isoalloxazine: ISC through a singlet-triplet crossing $(^3n_O\pi^*/^1\pi\pi^*)_{STC}$, relaxation on the $^3n_O\pi^*$ PEH, and IC toward the $^3(\pi\pi^*$ HL) state via a conical intersection $(^3\pi\pi^*/^3n_O\pi^*)_{CI}$ placed near the minimum of the $^3n_O\pi^*$ state, at 3.91 eV. Both the minimum and the CI have nearly planar structures in which the $C_4 = O$ bond length (see Figure 16-9) has been elongated to 1.36 Å from the initial FC geometry, 1.203 Å.

Apart from the previous mechanism, at 4.2 eV along the $^1(\pi\pi^*$ HL) MEP the $(^3\pi\pi^*/^1\pi\pi^*)_{STC}$ has been computed and thus connecting directly the initially populated state with T_1. The SOC in the STC point is obtained here much lower, $\sim$1 cm^{-1}, than in the other mechanism. The crossing is placed in the last part of the MEP, very close to the conical intersection of $^1(\pi\pi^*$ HL) with the ground state described in Section 16.2. The lowest triplet state may be populated from the conical intersection with the $^3(n_O\pi^*)$ state or via the singlet-triplet crossing with the $^1(\pi\pi^*$ HL) state. The MEP on $^3(\pi\pi^*)$ leads to the state minimum, $^3(\pi\pi^*)_{min}$, in which the molecule displays a distorted structure with an out-of-plane ring deformation and an increased length of the C_5C_6 bond to 1.503 Å. The high reactivity attributed to this triplet state originates from its biradical character on C_5 and C_6. The minimum is placed at 3.15 eV adiabatically (see Table 16-3) from the ground state optimized minimum, which can be compared with the 3.3 eV estimated for the location of the triplet state for uracil mononucleotide in aqueous solution at the room temperature [100]. It is also consistent with previous theoretical determinations at around 3.2 [101] and 3.1 eV [102]. The observed wavelength dependence of the intersystem

crossing quantum yield in uracil which is one order of magnitude larger at excitation energies near 5.4 eV than that near 4.4 eV can be interpreted by the contribution of both or just the lowest-energy ISC mechanisms, respectively.

As a final aspect of the evolution along the triplet manifold in uracil we have located the singlet-triplet crossing connecting the $^3(\pi\pi^*)$ and the ground state, and mapped the MEP leading from such STC toward $^3(\pi\pi^*)_{min}$. The crossing is placed at near 3.4 eV from the ground state minimum, which suggests that there is a barrier of 0.21 eV (4.7 kcal mol^{-1}) to reach $(gs/^3\pi\pi^*)_{STC}$ from $^3(\pi\pi^*)_{min}$. The molecule recovers there the planarity, and the computed electronic SOC is somewhat low, $\sim$1 cm^{-1}, predicting for the triplet state a long lifetime and a slow relaxation, becoming therefore prone to react. Unlike in the previous example, isoalloxazine, the phosphorescence detected in uracil or any of the other nucleobases is extremely weak [103]. In an earlier study, performed on the cytosine molecule [61], other mechanism for triplet population and deactivation was found, in particular that related with the distortion of the C=O bond length, leading to a conical intersection between the $^1(\pi\pi^*)$ and the ground state. As mentioned in Section 16.3 such CI can probably give rise to secondary energy deactivation paths in pyrimidine nucleobases. In general, the same type of distortion that destabilizes the ground state yielding a CI with the $^1(\pi\pi^*$ HL) state, leads to a singlet-triplet crossing between $^3(\pi\pi^*$ HL) and the ground state in the vicinity of the CI. This is the case for the ethene-like CI (or STC) described above in uracil and the CO-stretched CI (STC) computed in cytosine [3, 61]. SOC terms are however quite different in both cases. Whereas the computed SOC elements in the ethene-like STC region are close to 1 cm^{-1}, they reach 20–30 cm^{-1} near the CO-stretched STC, probably by the presence in the latter case of a nearby $n\pi^*$ state. Further refinements of these aspects will include the estimation of vibronic contributions to compute ISC rates [90].

16.5. BIOEXIMERS AS PRECURSOR OF CHARGE TRANSFER AND REACTIVITY IN PHOTOBIOLOGY

Many systems including rare gases, aromatic hydrocarbons, and nucleic acid bases form excimers and exciplexes. This statement might bring the following question: What is really meant by 'excimer'? The proper answer to this matter is somewhat long and can be found in the reviews on the topic [30, 104, 105]. Nevertheless, in order to be operative let us recall that an excimer was defined by Birks as "*a dimer which is associated in an excited electronic state and which is dissociative in its ground state*" [105]. In other words, the so-called excimer can be seen as a dimer where one of the partners is electronically excited but such a dimer immediately dissociates upon deexcitation. Strictly speaking, an exciplex is a similar complex but formed between two different molecules. Thus, it is really a heterodimer, although in the literature of DNA nucleobases the term excimer is commonly employed even if different bases are interacting [104]. We focus in this section on the study of certain excimers/exciplexes that are revealed to play a crucial role in mediating charge-transfer processes or that have been suggested as precursors of

DNA-bases photoproducts. Since the excimers (exciplexes) treated here are built from biological molecules, they hereafter shall be called generically bioexcimers (bioexciplexes). As an illustration of electron transfer (ET), the recent research [106] performed on the bioexciplex resulting from the interaction of reduced free base chlorin (FBC^-) and the *p*-benzoquinone molecule (Q) to yield neutral FBC and the *p*-benzosemiquinone radical anion (Q^-) is next summarized. As far as we are aware, this study can be classified as the first high-level ab initio prospective of *intermolecular* ET involving *neutral/reduced* species on realistic models related to the photosynthetic reaction centers (RCs). Apart from their own intrinsic interest, the results on the $[FBC/Q]^-$ bioexciplex give also the clues to understand the charge transfer process in DNA and related biopolymers, where the low-lying excited states of the oxidized and reduced bioexcimers built from similar and different nucleobases are implied [107]. On the other hand, reactivity of pyrimidines in the excited state leading to the formation of cyclobutane photoproducts shall be analyzed through cytosine. Computational evidence is given for the first time supporting the fact that the *singlet* and *triplet cytosine excimer* can both be unambiguously assigned as the precursors of the corresponding photoadducts, becoming relevant to fully understand the photoreactivity of cytosine along the singlet and triplet manifold [108].

The detailed knowledge of the key transformation processes responsible for transformation of solar energy into chemical energy in the photosynthetic RCs of bacteria, algae, and higher plants remains open as a challenging problem, from both experimental and theoretical standpoints. Research in this field may rapidly have a great impact in areas of current interest, especially in nanotechnology, material science, as well as the design of novel and friendly bioinspired devices. The underlying mechanism of ET occurring from reduced pheophytin ($Pheo^-$) to the primary stable photosynthetic acceptor, a plastoquinone (PQ) molecule, constitutes one of the most outstanding examples of ultrafast ET, which takes place in oxygenic photosynthesis. ET processes involving biochromophores are indeed quite often encountered in the corresponding biological functions in connection with the transduction of energy that ultimately leads to a biochemical signal and are usually described within the framework of the quasi-equilibrium Marcus' theory [109]. In photosynthesis, ETs have however two specific characteristics: (a) they are activationless, that is, they take place in the inverted region of the Marcus theory, and (b) they proceed very fast and in the same order of magnitude as the time scale of vibration motion (in the femto- or picosecond regime) and consequently nonequilibrium aspects have to be accounted for explicitly [110–112]. In order to make the computation manageable, the study has been focused on the following reaction:

$$FBC^- + Q \rightarrow FBC + Q^-.$$

As stated above, FBC/FBC^- represent the neutral/reduced forms of free base chlorin and Q/Q^- the *p*-benzoquinone molecule and *p*-benzosemiquinone radical anion, respectively.

Based on the computational evidence, it was concluded that the associated ultrafast ET reaction for the $[FBC/Q]^-$ bioexciplex can essentially be seen as a

radiationless transition mediated by a CI. Potential energy curves (PECs) for two low-lying doublet states of the $[FBC/Q]^-$ bioexciplex have been built along the intermolecular distance R for three different parallel arrangements, maintaining the structures fixed at the respective ground-state of the interacting moieties. The results obtained at the CASPT2 level employing the ANO-S C,N,O[3s2p1d]/H[2s] basis set are compiled in Figure 16-11. The active space for the reference CASSCF wave function comprised five MOs (four of FBC and one of Q) and five active electrons. It is really the minimum active space to describe the two different oxidation states of interest. The orientations considered are defined by the angle θ formed between the binary symmetry axis C_2 of FBC (perpendicular to the axis containing the inner pyrrolic hydrogen atoms) and the axis passing through the oxygen atoms of the Q molecule (cf. Figure 16-11). At each intermolecular distance recorded in the pictures, state-average CASSCF calculations of the lowest three roots were carried out for the bioexciplex at $\theta = 0°$ (C_s symmetry) and $\theta = 45°$ (C_1 symmetry), whereas two roots of each symmetry were computed for the $C_s\theta = 90°$ orientation. Just the lowest two roots have been collected in Figure 16-11.

At the infinite separation of the monomers, on the right-hand side of Figure 16-11, the energy difference between the two lowest states of the bioexciplex corresponds precisely to the energy difference of the vertical electron affinity computed for Q and FBC, about 0.7 eV, being the ($FBC^- + Q$) asymptotic limit above the lowest limit ($FBC + Q^-$). The CASSCF wave functions of $FBC^-$and Q^- are basically described by a single configuration with the extra electron located in the LUMO-like natural orbital. Structures that facilitate the overlap between the two LUMOs lead therefore to a more pronounced interaction and the occurrence of the state-crossing. Because of the overlap between the LUMOs decreases considerably at $\theta = 90°$, no crossing is computed for this orientation. On the contrary, the PECs do intersect at the other two orientations. The most effective interaction occurs at $\theta = 45°$, reflecting a larger overlap between the respective LUMOs. For this reason, when the two moieties get progressively closer, the crossing between the two curves appear earlier at $\theta = 45°$, at about 4 Å, with respect to $\theta = 0°$, at about 3.3 Å reflecting in the latter a somewhat less efficient interaction. Therefore, it is expected that the ET process becomes most efficient at $\theta = 45°$, associated to a relatively higher rate constant [111]. The actual crossing point should hopefully correspond to a CI and its geometry most probably should display for the FBC skeleton a distortion from the planarity. This finding reinforces previous suggestions on the role that crossing seams play in the ultrafast ET processes occurring ubiquitously in many biochemical systems. The curves in Figure 16-11 should however be interpreted with caution. They do not represent the ultrafast ET mechanism in RC but demonstrate that the involvement of CIs in the ET process is possible for certain donor-acceptor orientations. At short intermolecular distances the $FBC^- + Q$ system becomes the ground state, which is connected adiabatically to $FBC + Q^-$ at infinity. Depending on the topology of the actual CI, both minima may be populated. Ideally, such topology should be favoring population of the charge-transfer state ($FBC + Q^-$). A number of crossing and recrossings probably occur around the CI region leading to

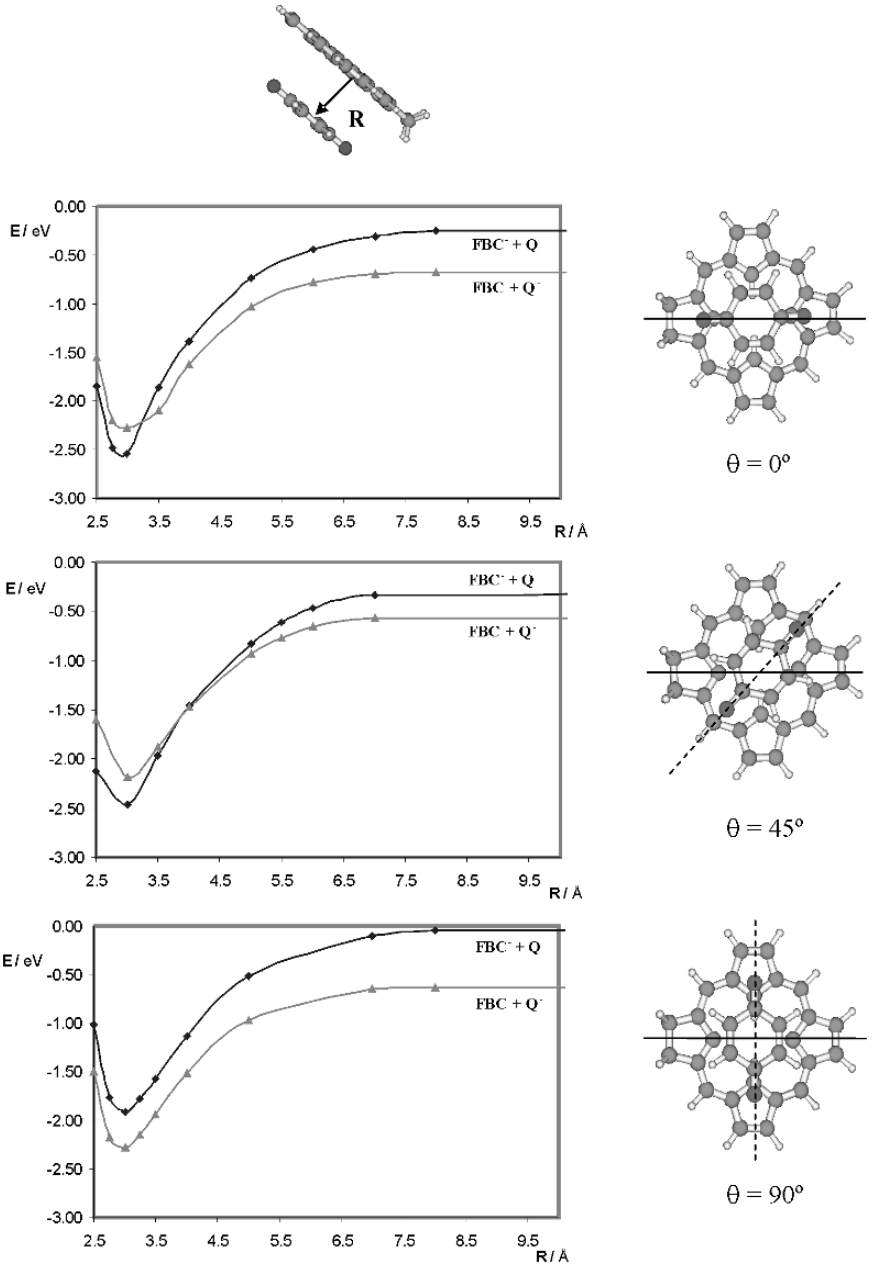

Figure 16-11. CASPT2 potential energy curves for the $[FBC/Q]^-$ system built with respect to the intermolecular distance R (see top). The three different orientations are defined by angle θ (see right-hand side and text). (Reproduced from Ref. [106] with permission from the American Chemical Society.)

the fulfillment of ET. By a subsequent increase of the intermolecular distance the products of the ET reaction, neutral FBC and reduced quinone Q^- are ultimately collected. The primary reduced quinone is then ready to transfer an electron to the secondary quinone and Pheo (FBC in our model) is willing to be involved again in new photoinduced charge-transfer process in the RCs. As discussed elsewhere [107] a similar scheme is useful in modeling charge transfer in DNA, which is evident from a recent work on the low-lying excited states of oxidized and reduced cytosine homodimer.

The UV irradiation of many microorganism leads to mutations and most of the occasions to lethal consequences [92, 95, 113]. Since the wavelength dependence of these biological effects has been shown to be identical with the absorption spectrum of DNA, photodamage produced in DNA centers may be responsible for mutagenesis. In the short interval between the absorption of a UV photon by one of the bases of DNA and the final formation of a photoproduct, many rearrangements can take place involving excited states of different multiplicities, energy may be transferred from different parts of DNA, and even some covalent bonds may be formed while others may be broken. Once the initial UV excitation has taken place, electronic states of DNA of different multiplicities, singlet (^{1}DNA*), doublet (^{2}DNA*), and triplet (^{3}DNA*) can be produced [114]. As Figure 16-12 illustrates, especially relevant for the photodimerization of pyrimidines are the low-lying singlet and triplet excited states. Thus, the scheme emphasizes that the two type of excited states, the lowest excited singlet and triplet states, are of greatest importance.

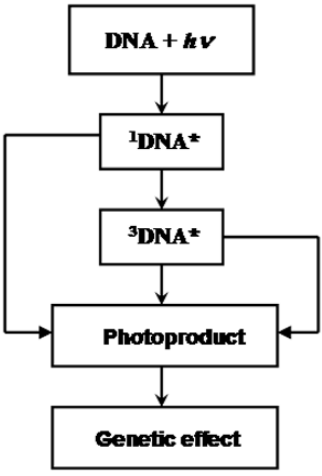

Figure 16-12. Schematic representation of the main paths of photoproduct formation, in particular photodimers of pyrimidines, through the singlet (^{1}DNA*) and triplet (^{3}DNA*) excited states once the energy is absorbed by DNA. The photolesion can ultimately lead to a genetic defect. (Adapted from Ref. [114].)

Light initially absorbed by nucleic acid bases leads mainly to excited states of the same multiplicity (singlet) as the respective ground state because singlet-to-singlet transition are dipole allowed whereas singlet-to-triplet absorption is spin forbidden. The excited state reaction along the singlet manifold occurs in competition with internal conversion processes to the electronic ground state. On the other hand, DNA triplet excited states may be populated through ISC mechanisms. During the last decade the role of triplet states in DNA chemistry, in particular on the formation of Pyr<>Pyr complexes, has been highlighted since it was first suggested by Cadet and co-workers [92]. Despite the fact that triplet formation has a low quantum yield, the longer-lived triplet states are crucial in the photochemistry and photophysics of DNA components, since they induce mutations at the bipyrimidine sites under triplet photosensitization conditions. Another route via triplet state Pyr-formation is also possible. Indeed, as it has been documented in detail for cytosine, along the ultrafast internal conversion, the lowest triplet state can be populated by an intersystem crossing (ISC) mechanism [61]. Still, the possibility of triplet energy transfer in DNA between different nucleobases is currently under study in our group. Apparently in contrast, recent time-resolved studies of thymine dimer formation by Marguet and Markovitsi [115] show that direct excitation of $(dT)_{20}$ leads to cyclobutane thymine dimers (T<>T) in less that 200 ns; remarkably any triplet absorption was not revealed from the transient spectra of the oligonucleotide. On the other hand, thymine dimerization has recently been determined by Schreier et al. [116] to be an ultrafast reaction along the singlet manifold, although no evidence for thymine excimers could be earlier recorded. It is clear that the origin and mechanisms of both excimer and photodimer formation at the molecular level are controversial and poorly understood.

One of the main motivations for studying the excited states of nucleic acids relies on the observation that UV illumination causes mutations due to photochemical modifications, the most common involving cycloaddition reactions of pyrimidines thymine and cytosine. Although the production of T-T cyclobutane dimers is most frequent, those involving C more often lead to mutation. The singlet excimer state has been suggested as a precursor to photodimerization by some authors [30, 95]. Excimer emission has indeed played an extensive role in the study of excited-state properties of nucleic acid polymers and oligomers, wherein the planar base molecules are staked upon excitation. Thus the term *static excimer* has been suggested in order to describe pairs of aromatic molecules which are in contact at the time of absorption [30]. The close proximity of the two chromophores in a system that forms *static excimers* can lead to changes in absorption and differences in fluorescence excitation spectra, two effects that are observed in base multimers. Thus, the profile of the absorption spectrum of double-stranded DNA closely resembles the sum of the absorption spectra of the constituent purine and pyrimidine bases but is about 30 per cent less intense [114]. Such a decrease of intensity is known as hypochromism. The fluorescence spectra of DNA and the constituent nucleotides are however qualitatively different. In fact, one intriguing aspect of UV-irradiated DNA is the appearance of red-shifted long-lived emissive states

not found in base monomers, which is observed for both the single- and double-stranded forms of polynucleotides. It is normally denoted in the literature as *excimer fluorescence,* a term firstly proposed by Eisinger et al. [117], reflecting the relevant role assumed to be played by the corresponding excited dimer (excimer) of the biopolymer. In general, excimers are observed almost exclusively by their characteristic fluorescence, which is shifted to longer wavelengths relative to the monomer fluorescence because of excited-state stabilization and ground-state destabilization. The recent time- and wavelength-resolved fluorescence study on different oligonucleotides reported by Plessow et al. [118] using 80 picoseconds (ps) excitation pulses makes readily apparent the longer-decay components and red-shifted emission that it was assumed to arise from excimer formation. In particular, for the cytosine (C) oligonucleotide 15-mer $d(C)_{15}$ a decay component of several nanoseconds (ns) is clearly observed as compared to the less intense feature of the dimer $d(C)_2$, and to the mononucleotide CMP, the latter showing a short instrument-limited decay. As mentioned above, because of the slow rate of energy relaxation, these long-lived states associated to excimer-like states have been suggested as the precursors of the DNA photolessions, including photodimers.

Surprisingly, despite that the existence of excimer- and exciplex-like excited states of nucleobases are invoked widely in the experimental literature, until very recently support from the high-level ab initio study was not available. Just a few months ago we were able to report an exhaustive study on the low-lying singlet excited states derived from the π-stacked face-to-face interaction of two cytosine molecules (see Figure 16-13, *top*) with respect to the intermolecular distance of the monomers by using high-level ab initio computations, keeping the geometry of the monomers at its ground-state equilibrium structure [119].

The accurate theoretical treatment of the resulting excimers is revealed to be particularly challenging since it requires the inclusion of electron dynamic correlation, flexible enough one-electron basis sets, wave functions with no symmetry constraints in order to achieve the correct asymptotic limit, and corrections for the basis set superposition error (BSSE). The present research supports that the excimer origin of the red-shifted fluorescence observed in the corresponding oligonucleotides of cytosine is an intrinsic property of the nucleobase dimer. Twelve active π electrons distributed among twelve π active orbitals were employed in the respective CASSCF(12,12) wave functions. By using the subsequently multiconfigurational second-order perturbation method CASPT2 (plus BSSE), the lowest-singlet excited state of the π-stacked cytosine homodimer has been predicted to be bound by 0.58 eV. The computed emissive feature was revealed to be at 3.40 eV [119] and this results is consistent with the available experimental data for dinucleotides, polynucleotides, and DNA (3.2–3.4 eV) [117, 118]. The photophysics of the cytosine homodimer involving the singlet excited states is depicted in Figure 16-13a. In addition, the CASPT2 results obtained from a parallel study carried out on the two lowest triplet states of the cytosine-cytosine system are shown in Figure 16-13b. The binding energy for the lowest triplet state computed at the CASPT2 level (plus BSSE) is 0.22 eV with a predicted vertical emission (phosphorescence) at 3.23 eV

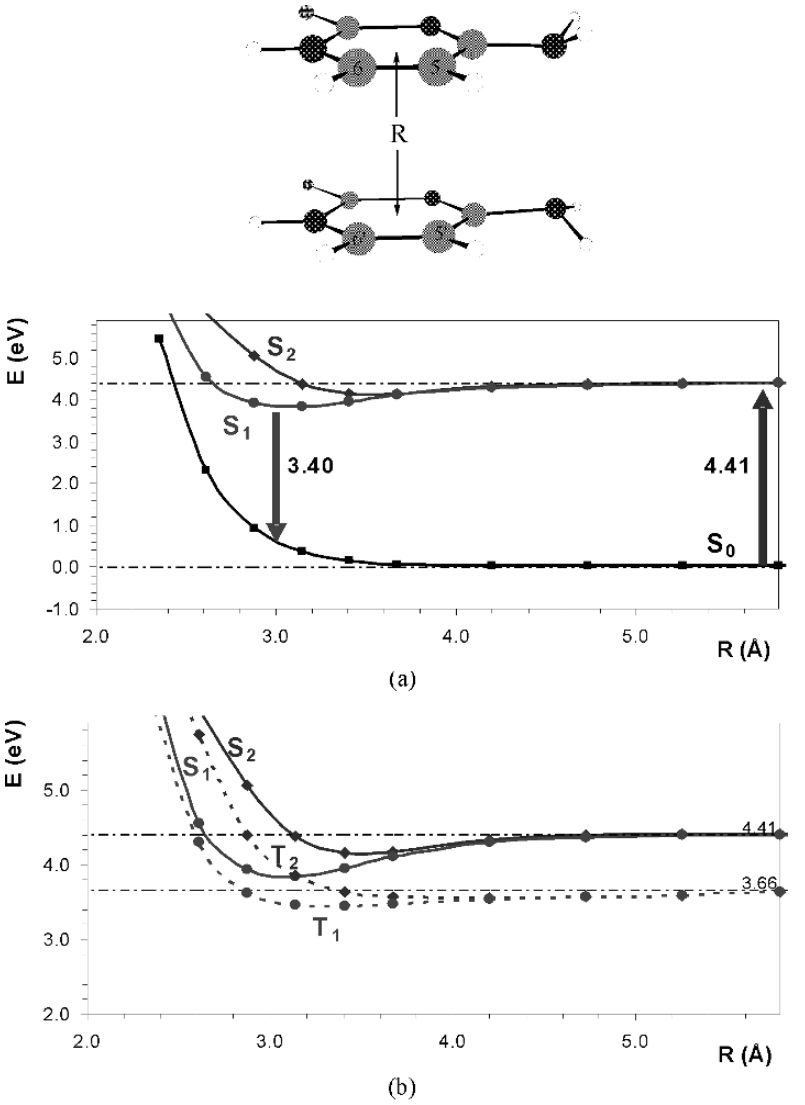

Figure 16-13. CASPT2(12,12)/ANO-S C,N,O[3s2p1d]/H[2s1p] potential energy curves built with respect to the intermolecular distance R(C5-C5') of two face-to-face π-stacked cytosine molecules involving the ground and the two lowest singlet excited states (a) and superimposing also the two lowest triplet excited states (b)

and a 0–0 triplet-singlet transition at 3.44 eV. Consequently, it is concluded that the triplet excimer is bound, although the binding energy is reduced about 60% with respect to singlet excimer. Interestingly, as can be noted from Figure 16-13b,

the S_1 and T_2 states are involved in a singlet-triplet crossing at an intermolecular distance of 3.0–3.4 Å, which precisely are the distances expected for the ground-state biopolymer. Thus, T_2 could be populated through ISC mechanism, becoming then deactivated toward T_1 via CI facilitated with the breathing movement of the own DNA. The possibility of excimer formation arises from the Watson-Crick structure in which hydrogen-bonded pairs A-T and G-C are situated inside a double helix backbone formed by two sugar-phosphate chains. One turn of the helix involves ten base pairs and is 34 Å high. Thus, the interplanar distance between neighboring base pairs is about 3.4 Å, a value which is often found in excimer-type organic crystals [105]. The structure for the locally excited state relative minimum on S_1 and T_1 computed at the CASPT2 level with respect to the intermolecular distance in the face-to-face arrangement (maintaining the monomers at the optimized ground-state geometry) shall be accordingly denoted as ^{1}(LE) and ^{3}(LE), respectively. For these structures the R(C5-C5′) distance is 3.076 and 3.304 Å. Taking into account the inherent flexibility of the DNA and related oligonucleotides, competitive ^{1}(LE)-type parallel orientations might be present at the time of UV-irradiation. Because of the increased stability of the lowest excited state, geometries around the ^{1}(LE)-type structure can be considered as the best candidates as precursors of photodimers. It seems that the ideal twist angle between successive base pairs makes the geometry of the B-DNA (and A-DNA) nonreactive. According to recent experimental evidence, the static Pyr-Pyr conformations and not conformational motions after photoexcitation determines the formation of (Pyr<>Pyr) photoproducts. Within the model proposed by Schreier et al. [116], the relatively smaller degree of flexibility of A-DNA compared to B-DNA to achieve the right orientations that become prone for photoreaction has been related to the greater resistance of A-DNA to (Pyr<>Pyr) formation. As shown by these authors, dimerization occurs only for thymine residues that are already in a reactive arrangement at the instant of excitation because the rate of formation by favorably oriented thymine pairs is much faster that the rate of orientation change. A similar situation can therefore be assumed in cytosine oligomers. From the results compiled so far, the ^{1}(LE)-type cytosine excimer is revealed as a reactive intermediate, possible source of the cyclobutane cytosine (CBC) dimer photoproduct, and consequently the ^{1}(LE) excimer has been taken as the starting point for the study of the dimerization reaction occurring along the singlet manifold. Similarly, the ^{3}(LE)-type cytosine excimer has been taking as the starting structure to study the reactivity of the system along the triplet manifold. It is should be however kept in mind that the magnitude of the spin-orbit coupling (SOC), which is directly related to the efficiency of the ISC process (see Section 16.4), would strongly be affected by the actual environment of the biopolymer.

The CASPT2 results on the photodimerization of two cytosine molecules taking place along the triplet manifold are compiled in Figure 16-14. As can be deduced from this figure that the MEP computations from ^{3}(LE) lead directly to the triplet step-wise intermediate ^{3}(SWI) with out any energy barrier. This intermediate (^{3}(SWI)) is characterized by the formation of a single covalent bond

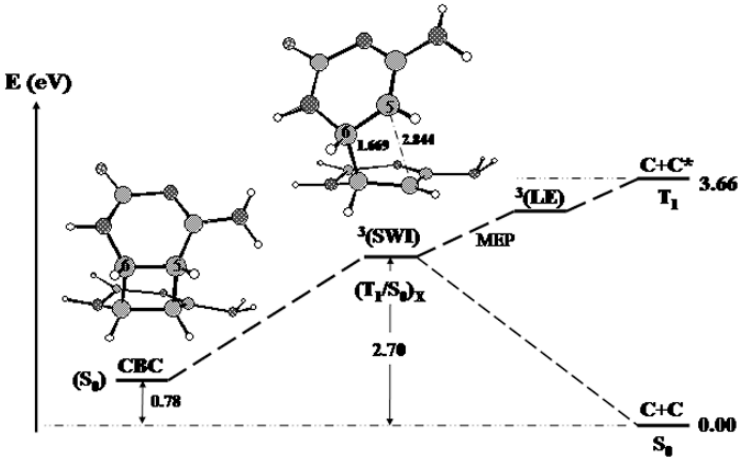

Figure 16-14. Computed energy levels for the ground state (S_0) and the lowest triplet excited state (T_1) of the cytosine dimer in its triplet locally excited state ^{3}(LE), step-wise intermediate ^{3}(SWI), and ground-state cyclobutane cytosine (CBC) dimer. The main intermolecular geometric parameters (in Å) for ^{3}(SWI) are included. At the ^{3}(SWI) optimized structure a singlet-triplet crossing, $(T_1/S_0)_X$, takes place

between the C_6-$C_{6'}$ with the bondlength of 1.669 Å, whereas the C_5-$C_{5'}$ interatomic distance remains elongated by about 2.8 Å. Remarkably, at the optimal structure of ^{3}(SWI) the ground state of the system becomes degenerate. In other words, the triplet state is coincident with a triplet-singlet crossing, $(T_1/S_0)_X$, which is a region of the hypersurface where decay to the ground state becomes particularly favored.

The singlet-triplet degeneracy occurring at the equilibrium structure ^{3}(SWI) can be understood on the basis of the biradical character of the triplet/singlet states, having the unpaired electrons located on the C_5 and $C_{5'}$ atoms, yielding also a rationalization for the relatively longer C_5-$C_{5'}$ distance with respect to that calculated for the C_6-$C_{6'}$. The ^{3}(SWI) structure cannot be considered an excimer but an intermediate toward the formation of CBC. The ^{3}(SWI) state lies 2.70 eV above the two ground-state cytosine molecules. The latter can be considered a lower bound for the triplet energy of cytosine and in DNA. It can be envisaged that exogenous photosensitizers could populate the relaxed triplet state of the monomer, which will subsequently evolve toward ^{3}(SWI) and then toward the formation of the mutated dimers. Thus, the required energy can be related to the threshold observed experimentally for a given compound to become a potential DNA photodamager via (C<>C) or (T<>T) formation. The computed result of 2.70 eV for the ^{3}(SWI) structure of cytosine is totally consistent with the triplet energy of thymine in DNA [108] deduced experimentally at 2.80 eV [120]. The intermediate labeled ^{3}(SWI) thus represents a channel for the photodimer formation from the triplet state of

π-stacked cytosine (and presumably also for thymine) in DNA and provides the basic understanding of potential phototogenotoxicity via triplet-triplet sensitization.

Ongoing work is in progress to elucidate the mechanism of the formation of cytosine photodimer along the singlet manifold. Taking into account the seminal work reported by Bernardi, Olivucci, and Robb in 1990 on predicting the forbidden and allowed excited-state [2+2] cycloadditon reactions of two ethene molecules [121], one would expect a CI toward the ground-state CBC from the relaxed singlet excimer. It is cl early verified so far that MEP computations from the ^{1}(LE) state lead to such stationary (relaxed) excimer. The process in the singlet manifold is also expected to follow a steepest descent path as it occurs along the triplet hypersurface, although further details on the mechanism have to wait until the CI structure is fully characterized. Thus, the current view supports the hypothesis that the dimerization photoreaction of two cytosine molecules occurs barrierless, both on the singlet and triplet hypersurfaces. It would depend on the experimental conditions whether the singlet or triplet mechanism becomes activated, fully operative or even competitive with each other. The different mechanisms proposed in the literature involve singlet and triplet states of the monomers and vertical stacking to account for dimerization in solution and solid state, respectively. These mechanisms are here supported on the basis of CASPT2 results. The efficiency of the photodimerization would markedly depend on the experimental conditions (solvent, aggregation conditions, pH, degree of hydratation), the sequence of nucleotides, and the type (A-, B- C-like) of DNA conformation [92, 116]. In fact, if dimer formation occurs with reasonable yields between monomeric solute molecules in solution, the dimer must have a triplet precursor, because singlet lifetimes simply are not long enough to permit excited bimolecular reactions [114]. Nevertheless, as Eisinger and Shulman have emphasized [114], the same reaction which proceeds via triplet state in solution may have a singlet-state precursor when the biochromophores are held together, as it is the case in frozen solutions or in a biopolymer. Theory predicts that the photoinduced reactions both on the singlet and triplet hypersurfaces are essentially barrierless and singlet and triplet excimers play an active role in the photophysical outcome and in the photochemical properties of cytosine-containing biopolymers. In particular, an *ultrafast* decay of the triplet state to yield the corresponding ground-state cyclobutane dimer is expected. The presence of $(T_1/S_0)_X$ crossing favors the ISC to the ground state, possibly taking place on a subpicosecond range, which is considerably less than the 200 ns employed in the time-resolved study of thymine dimer formation [115]. Therefore, the present results do fully support the suggestion made by Marguet and Markovitsi [115] in relation to the possibility that the ultrafast reactivity of the triplet state to yield cyclobutane dimers occurs with quasi unit efficiency. On the other hand, it does not contradict the experimental finding announced by Schreier et al. [116] that thymine dimerization in DNA occurring along the singlet manifold is an ultrafast photoreaction. The present results also offer a nice rationale to the known fact that pyrimidine dimers are formed under triplet photosensitization conditions [92].

16.6. SUMMARY AND CONCLUSIONS

The theoretical study of photophysical and photochemical problems requires an accurate determination of the complex potential energy hypersurfaces of the low-lying electronic excited states. The quantum chemical methods employed to compute reaction profiles, energy gaps, molecular structures, state crossings, and molecular properties must include effects of dynamical correlation in a balanced way. These effects if not included or wrongly accounted for, may provide a deficient view of the problem, for instance, erroneous profiles for the reaction paths or spurious state crossings or minima, leading in turn to fictitious reaction dynamics. In the present report we have illustrated in different cases that fully correlated ab initio methods like CASSCF/CASPT2 and large one-electron basis sets of the ANO type are frequently required in order to obtain accurate results which are not provided by lower-level strategies. Also, it has been here stressed the importance of not only properly locating conical intersections (CIs), protagonists of nonadiabatic photochemistry, but also the need of determining the accessibility of the seam of CIs as the cornerstone to understand the photochemical processes. Computation of minimum energy paths (MEPs) along the path of the energy has been proved to be the most accurate procedure to guarantee the absence of presence of energy barriers in the path for energy decay in the different systems.

Our attention here has been focused on the photochemistry of DNA/RNA base monomers upon absorption of UV radiation. Once the spectroscopic $\pi\pi^*$ singlet excited state, related with the HOMO $\rightarrow$ LUMO transition having the largest oscillator strength at low energies, has been populated, computed MEPs for the five natural nucleic acid bases, uracil, thymine, cytosine, adenine, and guanine, have been shown to lead the molecule in a barrierless way towards an out-of-plane ethene-like conical intersection connecting the initially excited and the respective ground state. Cytosine is an exception that has two competitive profiles leading toward the mentioned CI and a low-lying planar minimum. In either case, the barrierless path can be related to the ultrafast femtosecond decay measured in molecular beams for the five nucleobases, only slightly modified in condensed phases, for nucleosides or nucleotides. Slower picosecond decays and transfer to triplet states have been also measured. The present calculations provide the key aspects needed to formulate a general unified model to describe the photochemistry of the systems by properly computing MEPs, minima, and conical intersection between the different states. Singlet-triplet crossings have been also obtained and used to explain the efficient population of the low-lying reactive $\pi\pi^*$ triplet state of nucleobases and other biological molecules because of the presence of favorable intersystem crossings with the initially populated singlet states. Examples have been uracil, cytosine, and isoalloxazine, the favin core ring.

The importance of bioexcimers (bioexciplexes) in the photochemistry of biological compounds has been also emphasized. Computation of potential energy curves modeling the complex pheophytin-quinone shows the relevance that stabilization caused by the formation of π-stacked excited dimers, that is, excimers (exciplexes) and the corresponding presence of conical intersections, have to provide

channels for ultrafast electron transfer in photosynthetic centers. Maximization of the orbital overlap has been shown to be an important aspect to determine favorable orientations for the process to take place. In a similar fashion, the existence of singlet and triplet excimers in the cytosine dimer has been proved to explain: First, the presence of an additional fluorescence in the spectra of DNA, red-shifted with respect to the monomer fluorescence, the former originated by the excimer. Second, the excimer is suggested to be the precursor of the formation of the cyclobutane cytosine (CBC) dimer, one of the most frequent photolesions found in DNA after UV irradiation. The barrierless character of the path from the triplet excimer toward a singlet-triplet crossing connecting the lowest triplet and the ground CBC state, points toward a favorable dimerization process in the triplet manifold, also present along the singlet states and taking place through a corresponding conical intersection, as suggested by the calculations. In the present report we wanted to reflect the complexity of the photochemistry of biological compounds, trying to set the path for future, more complete, calculations which can be used to determine proper dynamics for the systems.

ACKNOWLEDGEMENTS

The authors want to thank the contributions of their co-workers in the different projects included in the present chapter. Also the efforts of the other developers of the MOLCAS code are deeply acknowledged. The authors do also want to acknowledge the contributions of other researchers, referees, and colleagues in the area of modern photochemistry, which has experienced recent and important developments and it will continue to grow only with a synergic cooperation. Financial support is acknowledged from projects CTQ2004-01739 and CTQ2007-61260 of the Spanish MEC/FEDER and GV06-192 of the Generalitat Valenciana, and from the European Science Foundation (ESF) through COST Action P9.

REFERENCES

1. Olivucci M (ed) (2005) Computational Photochemistry, Elsevier, Amsterdam.
2. Lawley, KP (ed) (1987) Ab Initio Methods in Quantum Chem.-II, Wiley, New York.
3. Merchán M, Serrano-Andrés L (2003) J Am Chem Soc 125:8108.
4. Serrano-Andrés L, Merchán M (2005) J Mol Struct Theochem 729:99.
5. Merchán M, Serrano-Andrés L (2005) Ab Initio Methods for Excited States. In: Olivucci M (ed) Computational Photochemistry, Elsevier, Amsterdam.
6. Robb MA, Olivucci M, Bernardi F (2004) Photochemistry. In: Schleyer PvR, Jorgensen WL, Schaefer HF, III, Schreiner PR, Thiel W, Glen R (eds) Encyclopedia of Computational Chemistry, Wiley, Chichester.
7. Klessinger M, Michl J (1995) Excited States and Photochemistry of Organic Molecules, VCH, New York.
8. Domcke W, Yarkony DR, Köppel H (eds) (2004) Conical Intersections, World Scientific, Singapore.

9. Michl J (2005) Ab Initio Methods for Excited States. In: Olivucci M (ed) Computational Photochemistry, Elsevier, Amsterdam.
10. De Vico L, Olivucci M, Lindh R (2005) J Chem Theory Comp 1:1029.
11. Anglada JM, Bofill JM (1997) J Comput Chem 18:992.
12. Müller K, Brown LD (1979) Theor Chim Acta 53:75.
13. Andersson K, Barysz M, Bernhardsson A, Blomberg MRA, Carissan Y, Cooper DL, Cossi M, Fülscher MP, Gagliardi L, De Graaf C, Hess B, Hagberg G, Karlström G, Lindh L, Malmqvist P-Å, Nakajima T, Neogrády P, Olsen J, Raab J, Roos BO, Ryde U, Schimmelpfennig B, Schütz M, Seijo L, Serrano-Andrés L, Siegbahn PEM, Stålring J, Thorsteinsson T, Veryazov V, Widmark PO (2004) *MOLCAS, version* 6.0. Department of Theoretical Chemistry, Chemical Centre, University of Lund, P.O.B. 124, S-221 00 Lund, Sweden.
14. Andersson K, Malmqvist P-Å, Roos BO, Sadlej AJ, Wolinski K (1990) J Phys Chem 94:5483.
15. Andersson K, Malmqvist P-Å, Roos BO (1992) J Chem Phys 96:1218.
16. Finley J, Mamqvist P-Å, Roos BO, Serrano-Andrés L (1998) Chem Phys Lett 288:299.
17. Serrano-Andrés L, Merchán M, Lindh R (2005) J Chem Phys 122:104107.
18. Forsberg N, Mamqvist P-Å (1997) Chem Phys Lett 274:196.
19. Serrano-Andrés L, Merchán M, Nebot-Gil I, Lindh R, Roos BO (1993) J Chem Phys 98:3151.
20. Roos BO, Fülscher MP, Malmqvist P-Å, Merchán M, Serrano-Andrés L (1996) Theoretical Studies of Electronic Spectra of Organic Molecules. In: Langhoff SR (ed) Quantum Mechanical Electronic Structure Calculations with Chemical Accuracy**,** Kluwer, Dordrecht, p 357.
21. Roos BO, Andersson K, Fülscher MP, Malmqvist P-Å, Serrano-Andrés L, Pierloot K, Merchán M (1996) Adv Chem Phys 93:219.
22. Merchán M, Serrano-Andrés L, Fülscher MP, Roos BO (1999) Multiconfigurational Perturbation Theory Applied to Excited States of Organic Compounds. In: Hirao K (ed) Recent Advances in Multireference Methods, World Scientific, Singapore, p 161.
23. González-Luque R, Garavelli M, Bernardi F, Merchán M, Robb MA, Olivucci M (2000) Proc Nat Acad Sci USA 97:9379.
24. Molina V, Merchán M (2001) Proc Nat Acad Sci USA 98:4299.
25. Serrano-Andrés L, Merchán M (2004) Spectroscopy: Applications. In: Schleyer PvR, Schreiner PR, Schaefer HF III, Jorgensen WL, Thiel W, Glen RC (eds) Encyclopedia of Computacional Chemistry, Wiley, Chichester, 2004.
26. Gagliardi L, Roos BO (2005) Nature 433:848.
27. Serrano-Andrés L, Merchán M, Borin AC (2006) Proc Nat Acad Sci USA 103:8691.
28. Strickler SJ, Berg RA (1962) J Chem Phys 37:814.
29. Rubio-Pons O, Serrano-Andrés L, Merchán M (2001) J Phys Chem A 105:9664.
30. Crespo-Hernández CE, Cohen B, Hare PM, Kohler B (2004) Chem Rev 104:1977.
31. Daniels M, Hauswirth WW (1971) Science 171:675.
32. Samoylova E, Lippert H, Ullrich S, Hertel IV, Radloff W, Schultz T (2004) J Am Chem Soc 127:1782.
33. Canuel C, Mons M, Piuzzi F, Tardivel B, Dimicoli I, Elhanine M (2005) J Chem Phys 122:074316.
34. Kuimova MK, Dyer J, George MW, Grills DC, Kelly JM, Matousek P, Parker AW, Sun XZ, Towrie M, Whelan AM (2005) Chem Commun 1182.
35. Fülscher MP, Roos BO (1995) J Am Chem Soc 117:2089.
36. Lorentzon J, Fülscher MP, Roos BO (1995) J Am Chem Soc 117:9265.
37. Fülscher MP, Serrano-Andrés L, Roos BO (1997) J Am Chem Soc 117:6168.
38. Shukla MK, Mishra PC (1999) Chem Phys 240:319.
39. Ismail N, Blancafort L, Olivucci M, Kohler B, Robb MA (2002) J Am Chem Soc 124:6818.
40. Sobolewski AL, Domcke W (2004) Phys Chem Chem. Phys 6:2763.

41. Matsika S (2004) J Phys Chem A 108:7584.
42. Kistler KA, Matsika S (2007) J Phys Chem A 111:2650.
43. Zgierski MZ, Patchkovskii S, Lim EC (2005) J Chem Phys 123:081101.
44. Zgierski MZ, Patchkovskii S, Fujiwara T, Lim EC (2005) J Phys Chem A 109:9384.
45. Tomic K, Tatchen J, Marian CM (2005) J Phys Chem A 109:8410.
46. Blancafort L, Cohen B, Hare PM, Kohler B, Robb MA (2005) J Phys Chem A 109:4431.
47. Merchán M, González-Luque R, Climent T, Serrano-Andrés L, Rodríguez E, Reguero M, Peláez D (2006) J Phys Chem B 110:26471.
48. Perun S, Sobolewski AL, Domcke W (2006) J Phys Chem A 110:13238.
49. Gustavsson T, Banyasz A, Lazzarotto E, Markovitsi D, Scalamani G, Frisch MJ, Barone V, Improta R (2006) J Amer Chem Soc 128:607.
50. Serrano-Andrés L, Merchán M, Borin AC (2006) Chem Eur J 12:6559.
51. Blancafort L (2006) J Am Chem Soc 128:210.
52. Marian CM (2005) J Chem Phys 122:104314.
53. Perun S, Sobolewski AL, Domcke W (2005) J Am Chem Soc 127:6257.
54. Chen H, Li SH (2005) J Phys Chem A 109:8443.
55. Chen H, Li SH (2006) J Chem Phys 124:154315.
56. Marian CM (2007) J Phys Chem A 111:1545.
57. Sobolewski AL, Domcke W (2002) Eur Phys J D 20:369.
58. Perun S, Sobolewski AL, Domcke W (2005) Chem Phys 313:107.
59. Truhlar DG, Mead CA (2003) Phys Rev A 68:032501.
60. Dreuw A, Worth GA, Cederbaum LS, Head-Gordon M (2004) J Phys Chem B 108:19049.
61. Merchán M, Serrano-Andrés L, Robb MA, Blancafort L (2005) J Am Chem Soc 127:1820.
62. Serrano-Andrés L, Merchán M, Borin AC (2008) J Am Chem Soc In press.
63. Hauswirth W, Daniels M (1971) Chem Phys Lett 10:140.
64. Callis PR (1979) Chem Phys Lett 61:563.
65. Callis PR (1983) Ann Rev Phys Chem 34:329.
66. Hare PM, Crespo-Hernández CE, Kohler B (2007) Proc Nat Acad Sci USA 104:435.
67. Marian CM (2007) J Phys Chem A 111:1545.
68. Choi MY, Miller RE (2006) J Am Chem Soc 128:7320.
69. Shukla MK, Leszczynski J (2006) Chem Phys Lett 429:261.
70. Chin W, Monsa M, Dimicoli I, Piuzzi F, Tardivel B, Elhanine M (2002) Eur Phys J D 20:347.
71. Colominas C, Luque FJ, Orozco M (1996) J Am Chem Soc 118:6811.
72. Klessinger M (1998) Triplet Photoreactions. Structural Dependence of Spin-orbit Coupling and Intersystem Crossing in Organic Biradicals. In: Párkányi C (ed) Theoretical Organic Chemistry–Theoretical and Computational Chemistry, Elsevier, Amsterdam, p 581.
73. Sidman JW (1958) J Mol Spectros 2:333.
74. Goodman L, Krishna VG (1963) Rev Mod Phys 35:541.
75. Hall WR (1976) Chem Phys Lett 37:335.
76. Bendazzoli GL, Palmieri P (1974) Int J Quantum Chem 8:941.
77. Langhoff SR (1974) J Chem Phys 61:1708.
78. Bendazzoli GL, Orlandi G, Palmieri P (1977) J Chem Phys 67:1948.
79. Lower SK, El-Sayed MA (1966) Chem Rev 66:199.
80. El-Sayed MA (1968) Acc Chem Res 1:8.
81. Crovetto L, Braslavsky E (2006) J Phys Chem A 110:7307.
82. Kowalczyk RM, Schleicher E, Bittl R, Weber S (2004) J Am Chem Soc 126:11393.
83. Climent T, González-Luque R, Merchán M, Serrano-Andrés L (2006) J Phys Chem A 110:13584.
84. Turro NJ (1991) Modern Molecular Photochemistry, University Science Books, Sausalito.

85. Shüttrigkeit TA. Kompa, CK, Salomon M, Rüdiger W, Michel-Beyerle ME (2003) Chem Phys 294:501.
86. Sun M, Moore TA, Song P-S (1972) J Am Chem Soc 94:5.
87. Visser AJWG, Müller F (1979) Helv Chim Acta 62:593.
88. Serrano-Pérez JJ, Serrano-Andrés L, Merchán M (2006) J Chem Phys 124:124502.
89. Serrano-Pérez JJ, Merchán M, Serrano-Andrés L (2007) Chem Phys Lett 434:107.
90. Tatchen J, Marian CM (2006) Chem Phys Phys Chem 8:2133.
91. Climent T, González-Luque R, Merchán M, Serrano-Andrés L (2007) Chem Phys Lett 441:327.
92. Cadet J, Vigny P (1990) The Photochemistry of Nucleic Acids. In: Morrison H (ed) Bioorganic Photochemistry, Wiley, New York.
93. Brown IH, Johns HE (1968) Photochem Photobiol 8:273.
94. Beukers R, Ijlstra J, Berends W (1960) Rev Trav Chim Pays Bas 79:101.
95. Danilov VI, Slyusarchuk ON, Alderfer JL, Stewart JJP, Callis PR (1994) Photochem Photobiol 59:125.
96. Leszczynski J (ed) (1999) Computational Molecular Biology, Elsevier, Amsterdam.
97. Ericsson LA (ed) (2001) Theoretical Biochemistry. Processes and Properties in Biological Systems, Elsevier, Amsterdam.
98. Sztumpf-Kulikowska E, Shugar D, Boag JW (1967) Photochem Photobiol 6:41.
99. Whillans DW, Johns HE (1969) Photochem Photobiol 6:323.
100. Wood PD, Redmond RW (1996) J Am Chem Soc 118:4256.
101. Marian CM, Schneider F, Kleinschmidt M, Tatchen J (2002) Eur Phys J D 20:357.
102. Nguyen MT, Zhang R, Nam P-C, Ceulemans A (2004) J Phys Chem A 108:6554.
103. Görner H (1990) J Photochem Photobiol B: Biol 5:359.
104. Klöpffer W (1973) Intramolecular Excimers. In: Birks JB (ed) Organic Molecular Photophysics, Interscience, London, p 35.
105. Birks JB (1975) Rep Prog Phys 38:903.
106. Olaso-González G, Merchán M, Serrano-Andrés L (2006) J Phys Chem B 110:24734.
107. Roca-Sanjuán D, Serrano-Andrés L, Merchán M (2008) Chem Phys In press.
108. Roca-Sanjuán D, Olaso-González G, González-Ramírez I, Serrano-Andrés L, Merchán M (2008) J Am Chem Soc In press.
109. Marcus RA (1964) Annu Rev Phys Chem 15:155.
110. Dreuw A, Worth GA, Cederbaum LS, Head-Gordon M (2004) J Phys Chem B 108:19049.
111. Barbara PF, Meyer TJ, Ratner AM (1996) J Phys Chem 100:13148.
112. Blancafort L, Jolibois F, Olivucci M, Robb MA (2001) J Am Chem Soc 123:722.
113. Kramer KH (1997) Proc Natl Acad Sci USA 94:11.
114. Eisinger J, Shulman RG (1968) Science 161:1311.
115. Marguet S, Markovitsi D (2005) J Am Chem Soc 127:5780.
116. Schreier WJ, Schrader TE, Koller FO, Gilch P, Crespo-Hernández CE, Swaminathan VN, Carell T, Zinth W, Kohler B (2007) Science 315:625.
117. Eisinger J, Guéron M, Shulman RG, Yamane T (1966) Proc Natl Acad Sci USA 55:1015.
118. Plessow R, Brockhinke A, Eimer W, Kohse-Höinghaus K (2000) J Phys Chem B 104:3695.
119. Olaso-González G, Roca-Sanjuán D, Serrano-Andrés L, Merchán M (2006) J Chem Phys 125:231102.
120. Bosca F, Lhiaubet-Vallet V, Cuquerella MC, Castell JV, Miranda MA (2006) J Am Chem Soc 128:6318.
121. Bernardi F, Olivucci M, Robb MA (1990) Acc Chem Res 23:405.